Received: 16 September 2022 | Accepted: 20 January 2023

DOI: 10.1111/ede.12429

RESEARCH ARTICLE

WILEY

# Morphological and temporal variation in early embryogenesis contributes to species divergence in Malawi cichlid fishes

**Aleksandra Marconi** | **Cassandra Zie Yang** | **Samuel McKay** | **M. Emília Santos**

Department of Zoology, University of Cambridge, Cambridge, UK

**Correspondence**
Aleksandra Marconi and M. Emília Santos, Department of Zoology, University of Cambridge, Cambridge, UK.
Email: am2510@cam.ac.uk and es754@cam.ac.uk

**Funding information**
Natural Environment Research Council; Wellcome Trust

**Abstract**

The cichlid fishes comprise the largest extant vertebrate family and are the quintessential example of rapid "explosive" adaptive radiations and phenotypic diversification. Despite low genetic divergence, East African cichlids harbor a spectacular intra- and interspecific morphological diversity, including the hyper-variable, neural crest (NC)-derived traits such as coloration and craniofacial skeleton. Although the genetic and developmental basis of these phenotypes has been investigated, understanding of when, and specifically how early, in ontogeny species-specific differences emerge, remains limited. Since adult traits often originate during embryonic development, the processes of embryogenesis could serve as a potential source of species-specific variation. Consequently, we designed a staging system by which we compare the features of embryogenesis between three Malawi cichlid species—*Astatotilapia calliptera*, *Tropheops* sp. 'mauve' and *Rhamphochromis* sp. "chilingali"—representing a wide spectrum of variation in pigmentation and craniofacial morphologies. Our results showed fundamental differences in multiple aspects of embryogenesis that could underlie interspecific divergence in adult adaptive traits. First, we identified variation in the somite number and signatures of temporal variation, or heterochrony, in the rates of somite formation. The heterochrony was also evident within and between species throughout ontogeny, up to the juvenile stages. Finally, the identified interspecific differences in the development of pigmentation and craniofacial cartilages, present at the earliest stages of their overt formation, provide compelling evidence that the species-specific trajectories begin divergence during early embryogenesis, potentially during somitogenesis and NC development. Altogether, our results expand our understanding of fundamental cichlid biology and provide new insights into the developmental origins of vertebrate morphological diversity.

**KEYWORDS**
cichlid embryonic development, craniofacial skeleton, heterochrony, pigmentation, somitogenesis

## 1 | INTRODUCTION

The cichlid fishes are a quintessential example of rapid "explosive" adaptive radiation and phenotypic diversification (Genner & Turner, 2005; Henning & Meyer, 2014; Kocher, 2004; Meyer, 1993; Meyer et al., 1990; Salzburger, 2018). Among cichlid radiations, the most species-rich are the multiple radiations in the Great Lakes of East Africa—Victoria, Malawi, and Tanganyika—where hundreds of species evolved in a remarkably short time span (Kocher, 2004). Despite the relative genomic homogeneity (Kocher, 2004; Loh et al., 2008; Malinsky et al., 2018; Moran & Kornfield, 1993), cichlids harbor a spectacular intra- and interspecific diversity in physiology, morphology, behavior, and ecological specialization, rendering them an attractive model system in a wide range of research fields.

Recent years have brought major efforts toward elucidating the genetic and developmental basis of cichlid morphological diversity. Akin to other vertebrates, a considerable proportion of cichlid phenotypic variation involves structures derived from a common progenitor cell population—the neural crest (NC) (Bronner & LeDouarin, 2012; Bronner & Simões-Costa, 2016). These embryonic multipotent cells arise at the dorsal side of the forming neural tube and migrate away to often distant regions of the embryo where they differentiate into a plethora of cell types. Among these are the elements of the peripheral nervous system, pigment cells, and craniofacial cartilages and bones (Douarin & Kalcheim, 1999). The NC-derived phenotypes that received most attention in cichlids are their distinctive pigmentation patterns (Albertson et al., 2014; Brzozowski et al., 2012; Hendrick et al., 2019; Kratochwil et al., 2018, 2022; Liang et al., 2020; Roberts et al., 2017; Santos et al., 2014), and the dramatic variation in craniofacial morphologies, associated with the divergent trophic strategies (Albertson & Kocher, 2006; Conith et al., 2018; Powder & Albertson, 2016; Powder et al., 2014, 2015).

Insights into the genetic basis of cichlid traits have been possible due to their experimental tractability, including the viability of hybrid crosses and amenability to genetic manipulations such as CRISPR-Cas9 (Albertson & Kocher, 2006; Clark et al., 2022; Juntti et al., 2013; Kocher, 2004; Li et al., 2021; Powder & Albertson, 2016). Despite these advances, the cellular and developmental mechanisms underlying cichlid morphological diversification remain unknown. One of the unanswered questions is exactly when and how species-specific phenotypes emerge during development between such closely related species?

Adult morphologies often originate during early embryonic development, hence the processes of embryogenesis could serve as a potential source of species-specific variation. Since NC development (and thus origins of both pigmentation patterns and craniofacial skeleton) coincides with the processes of gastrulation, neurulation, and somitogenesis in teleosts (Rocha et al., 2020), how conserved are these stages among cichlids? What are the species-specific and species-generic (i.e., shared by the clade) features of embryonic development?

Species-specific differences could result from variation in embryonic morphology at these early stages of ontogeny, as well as from changes in the timing, duration, or rate of developmental processes (i.e., heterochronies) (Alberch et al., 1979; McKinney & McNamara, 1992). To date, heterochronic shifts have been found to contribute to phenotypic divergence in several systems. For example, in Darwin's Finches, the gene *bmp4* shows variation in its timing and levels of expression, resulting in divergent beak morphologies that are locally adapted to different food sources (Abzhanov et al., 2004). Further, differences in the timing of expression of early regionalization genes at the onset of gastrulation underlie differences in brain morphology between *Astyanax mexicanus* surface and cavefish morphs (Torres-Paz et al., 2019). Such studies demonstrate the importance of early developmental heterochronies to organismal diversification and adaptation to the surrounding environments. Similar processes may also underlie the vast cichlid morphological diversity.

Temporal variation could be especially consequential when occurring in the periods of embryogenesis that are concomitant with NC development (e.g., somitogenesis). These differences could in turn potentially influence the timings of cranial and trunk NC cell (NCC) migration and the later formation of its derivatives (e.g., cartilage and pigment cell differentiation). To test if such embryonic stages show heterochronic divergence between cichlids, we characterize the early and late embryonic development of three closely related, yet morphologically distinct, Malawi cichlid species harboring

variability in NC-derived traits, such as craniofacial shape and pigmentation.

To date, the general features of embryonic development have been described in a handful of African cichlids, including *Labeotropheus*, *Oreochromis niloticus*, *Dimidiochromis compressiceps, Copadichromis azureus, Hemichromis bimaculatus, Haplochromis piceatus*, and *Astatotilapia burtoni* (Jones, 1972; Balon, 1977; de Jong et al., 2009; Fujimura & Okada, 2007; Hendrick et al., 2019; Woltering et al., 2018), yet only a few studies have explicitly compared developmental variation in early ontogeny between or within species (Jones, 1972; de Jong et al., 2009), with most being limited to a specific morphological trait (e.g., Hendrick et al., 2019; Powder et al., 2015).

Here, we provide a staging guide by which we compare the features of embryogenesis between three mouthbrooding Malawi cichlid species—*Astatotilapia calliptera* (AC), *Tropheops* sp. 'mauve' (TM), and *Rhamphochromis* sp. 'chilingali' (RC)—representing a wide spectrum of morphological variation in pigmentation and craniofacial shape (Figure 1a,c,d). TM has the characteristic "flattened" head shape of an algae grazer, RC has the elongated narrow jaws of a pelagic predator, and AC shows an intermediate phenotype of an omnivore generalist. The differences in body coloration involve distinct pigment pattern motifs, from vertical bars in TM, horizontal stripes of RC to melanic patches in AC, with the latter comprising features of both bars and stripes. To examine the developmental variation at both intra- and interspecific levels, we have included two populations of AC diverging in body coloration (main lake 'Salima' and riverine 'Mbaka'; Figure 1a,b) in our study system. The 'Mbaka' fish of both sexes are noticeably darker than their conspecifics from the "Salima" population. Craniofacial skeleton and pigmentation aside, the characterization and comparison of developmental processes between these species could be of interest for future morphological evolution studies due to their positions in the Malawi cichlid phylogeny.

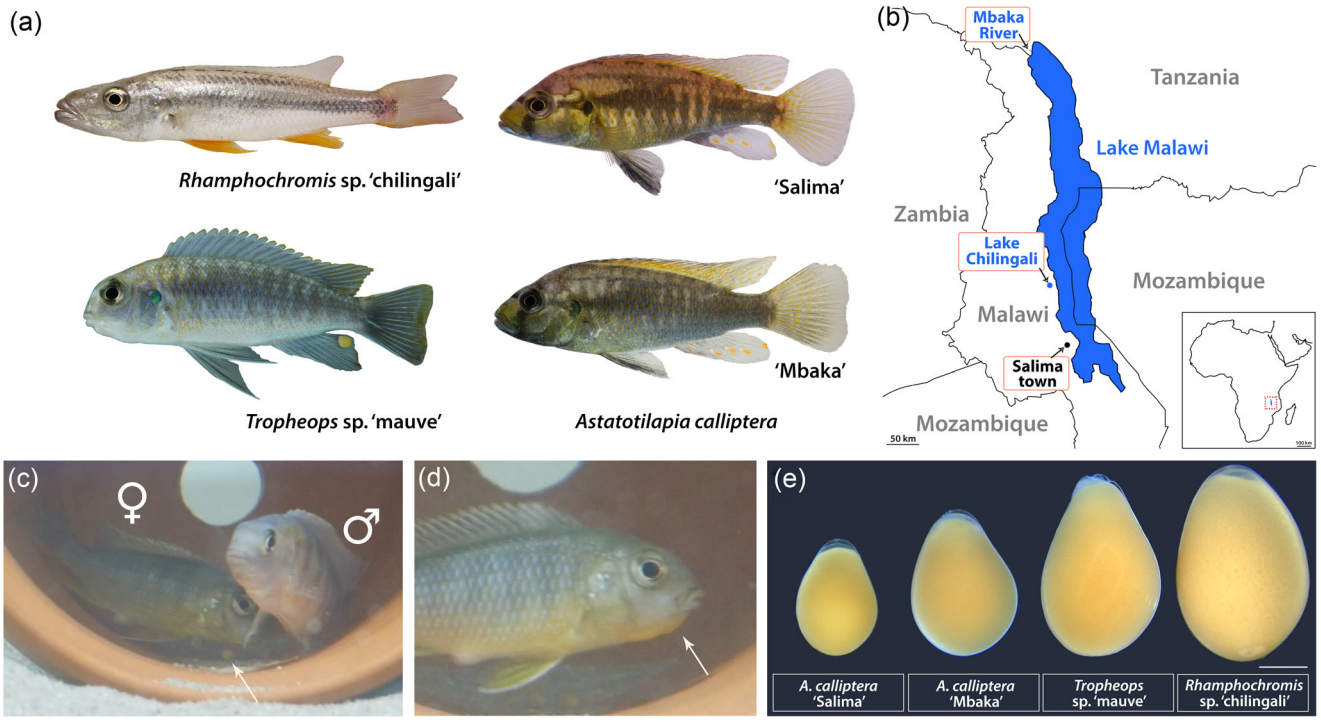


**FIGURE 1** Lake Malawi cichlids. (a) The four focal species of the study are characterized by clear variation in body coloration and craniofacial morphologies. *Rhamphochromis* are pelagic predators of other fish and arthropods and *Tropheops* are algae grazers, whereas the generalist *Astatotilapia calliptera* is considered to closely correspond to the common ancestor of the Malawi radiation (Malinsky et al., 2018). Note the difference in hue between the two populations of *A. calliptera*: "Salima" inhabiting the main lake reservoir and riverine "Mbaka." All individuals depicted are adult males; (b) All cichlids in the study are endemic to the Lake Malawi basin in East Africa, including Lake Chilingali and River Mbaka, located in close proximity to the main lake. Geographical boundaries drawn after Google Earth 2022; (c) *Tropheops* male and female pair during their courtship behavior. Note an egg underneath the female (white arrow); (d) Mouthbrooding female with a characteristic protruding "chin" (white arrow). (e) Diversity of egg sizes across the study species, implicating potential variation in the maternal provisioning (Supporting Information: Figure S1). Scale bar in $E = 1$ mm.

Notably, AC is thought to strongly resemble the prototype species of the entire radiation in terms of its ecology and phenotype (Malinsky et al., 2018).

We first present an overview of the development of these four cichlid fishes as a staging system. Further, we also examine in detail the timelines associated with early embryogenesis occurring concomitantly with the NC development (neurulation and somitogenesis). Finally, we summarize the earliest stages of the formation of the craniofacial skeleton and compare the timing and order of appearance of three pigment cell types contributing to the adult coloration (black melanophores, reflective iridophores, and yellow–orange xanthophores) altogether addressing the question of how early these NC-derived traits diverge in overt morphology. In addition to advancing our understanding of the timing of major developmental events and morphological divergence in early ontogeny, the resulting staging series will provide a valuable addition to the growing interest in cichlid evolutionary developmental biology and facilitate effective experimental design, including comparisons with other teleost systems.

## 2 | MATERIALS AND METHODS

### 2.1 | Animal husbandry and embryo culture

AC, RC, and TM were kept under standardized conditions (26 ± 1°C on a 12:12-h light cycle). These species are mouthbrooders (Figure 1c,d). To minimize the influence of maternal care, eggs were removed after fertilization. Since mating took from 30 min to 3 h, we considered the time of fertilization as approximately within the 1-h window from the first laid egg. Eggs were cultured individually in 1 mg/L of methylene blue (Sigma Aldrich) in water in six-well plates (ThermoFisher Scientific) placed on an orbital shaker moving at slow speed at 27°C. All experiments were conducted in compliance with the UK Home Office regulations.

### 2.2 | Staging system

Our staging (Supporting Information: Table S1) is based on the tables for *Astatotilapia burtoni* (Woltering et al., 2018), *Oreochromis niloticus* (Fujimura & Okada, 2007), and *Danio rerio* (Kimmel et al., 1995). We followed the definition proposed by Kratochwil et al. (2015) to measure epiboly as "the ratio between distances between the animal pole and blastoderm margin, and between the animal and vegetal pole." Embryo age is given in days, counting from the day of fertilization (Day 0).

### 2.3 | Imaging of live animals and fixed embryos

#### 2.3.1 | Adult animals

Adult photographs (Figure 1) were acquired with a Sony α6600 with a Sony E 30 mm f/3.5 lens.

#### 2.3.2 | Live embryos

For each species and stage reported in the staging (Figures 2 and 5–7) and head pigmentation development (Figure 11) series, several embryos ($n \geq 5$) from different clutches were examined and followed daily (Supporting Information: Table S2). For stages following hatching, live animals were imaged following anesthetization with MS-222 (800 mg/L, Sigma).

To observe the morphology of early embryos more closely, 0.6% v/v solution of dextran labeled with TexasRed (3000 MW, ThermoFisher Scientific) was injected at one-cell stage in AC eggs using a microinjector system (Applied Scientific Instrumentation). All live embryos (including those injected with TexasRed) were placed in glass-bottomed dishes (Cellvis) in 0.5% low melting point agarose (Promega) for imaging in brightfield (Figures 1e, 2, 5–7, and 11) or under RFP fluorescence (Figure 3). Images were taken through water to eliminate glare using a Leica M165FC and a Leica DFC7000T camera. Cameras were color balanced with a grey card (Grey White Balance Colour Card 24 by gwbcolourcard.uk). Using Adobe Photoshop 2022, multiple focal planes of stereoscopic images were aligned and merged, and any background imperfections were removed. Images of freshly fertilized eggs were used to infer the egg volume (Supporting Information: Figure S1) using "Egg Tools" plugin (https://www.jolyon.co.uk/myresearch/image-analysis/egg-shape-modelling) for Fiji (Schindelin et al., 2012).

#### 2.3.3 | Fixed specimens

Due to the limited access to one-cell TM and RC embryos, an alternative approach was applied: for each time point, embryos were dechorionated and dissected from yolk and fixed overnight at 4°C in 4% paraformaldehyde in 1X phosphate buffered saline (PBS). Samples were rinsed in 1X PBST (PBS + 0.01% Tween-20)

(20 min/rinse, twice) and stained with 10 nM DAPI (4′, 6-diamidino-2-phenylindole) (ThermoFisher Scientific) in 1X PBST overnight at 4°C. The embryos were rinsed twice with 1X PBST and mounted on glass-bottomed dishes (Cellvis) with ProLong™ Gold Antifade Mountant (ThermoFisher Scientific). A similar approach was applied to AC embryos used to determine the rates of somitogenesis (Supporting Information: Table S2). DAPI stainings were imaged with an Olympus FV3000. Confocal micrographs were stitched using the Olympus FV3000 software and processed with Fiji (Schindelin et al., 2012) to produce optical sections, collapse z-stacks and adjust image brightness and contrast where necessary. The same software used to measure the total embryo length, defined as the distance between the most anterior and posterior tip of the embryo, across segmentation (Supporting Information: Figure S3). All images were processed for background imperfections in Adobe Photoshop 2022, whereas graphs and statistical analyses were made using R version 4.1.1 (R Core Team, 2022).

## 2.4 | Histological sections

Embryos were cleared with histosol (National Diagnostics) (20 min/wash, three times) at room temperature and transitioned into wax in a 1:1 molten paraffin:histosol solution (30 min/wash, twice) and placed in molten paraffin (RA Lamb Wax; Fisher Scientific) at 60°C overnight. Molten paraffin was then changed five times (each change lasting >1 h) before the tissue was transferred into a Peel-A-Way embedding mold (Sigma) for transverse sectioning. The embedded blocks were left to cool overnight and sectioned using a Leica RM2125 RTS microtome. Sections were mounted on Superfrost plus slides (VWR). The paraffin-embedded sections were dewaxed in histosol (5 min/rinse, twice), 100% ethanol (5 min/rinse, twice) and grading into water through a series of descending ethanol concentrations (90%, 70%, and 50%, 5 min/rinse), followed by a final rinse in water (5 min). The slides were coverslipped with Fluoromount G containing DAPI (Southern Biotech) and cured overnight before imaging. The fluorescent micrographs were taken with Zeiss Axioscope A1 and combined into figure plates in Adobe Photoshop 2022.

## 2.5 | Cartilage preparations

Specimens were fixed overnight at 4°C in 4% paraformaldehyde in 1X PBS and dehydrated in increasing increments of ethanol:PBS (20%, 50%, and 70%; 10 min/wash) and stored in 70% ethanol:PBS at −20°C. The embryos were then transferred directly into 30% glacial acetic acid in ethanol and incubated for 2 h. Next, they were washed in Alcian Blue solution (0.02% Alcian Blue in acetic ethanol) for 2 h and incubated overnight in acetic ethanol. Next, the embryos were stepwise rehydrated from 30% acetic ethanol via 70%, 50%, 25% ethanol:di$H_2O$ (15 min/wash). The samples were then bleached in 2% KOH:3% $H_2O_2$ solution to remove skin pigmentation until melanophores turned from black to brown (2–16 h) and placed into 0.01% Alizarin Red in 1% KOH for 2 h. The specimens were cleared in 3:1 1% KOH:glycerol solution for 1–3 days, depending on the size of the animal. The solution was changed daily until the samples were sufficiently clear. Samples were subsequently transferred to 1:1 solution of 1% KOH:glycerol for 24 h and then placed in 1:3 solution of 1% KOH:glycerol until all Alizarin red cleared from non-ossified tissues (replaced with fresh solution daily, 1–3 days). Finally, the specimens were transferred to 80% glycerol for imaging and storage at 4°C. All washes were done with rocking and at room temperature. All cartilage preparations were carried out on at least six separate stage-matched individuals. The specimens were positioned in 100% glycerol in glass-bottomed dishes (Cellvis) and imaged using a Leica M165FC with Leica DFC7000T camera. The images were color-corrected in Adobe Photoshop 2022.

## 2.6 | Geometric morphometrics

To analyse the lateral and ventral development, the positions of homologous anatomical landmarks were collected from images using TPSUtil and TPSDig2 (Rohlf, 2010) following modified landmark protocol of Powder et al. (2015) (Supporting Information: Figure S2). MorphoJ (Klingenberg, 2011) was used to perform a generalized Procrustes analysis on the landmark coordinate data to exclude any other sources of variation than shape. This software was also used to generate covariance matrices and perform a principal components analysis (PCA) (Supporting Information: Figure S4). All specimens (Supporting Information: Table S3) were staged following definitions detailed in Supporting Information: Table S1 to avoid the potentially confounding effects of developmental heterochrony when using solely chronological age. We analysed the samples as follows: (1) across the species' ontogenies (st. 18–20) (Figure 10) and (2) among stage-matched individuals across all species (i.e., at single developmental time point, Supporting Information: Figure S5). To identify differences among these groups, we used canonical variate

analysis (CVA) across 10,000 iterations per comparison using Mahalanobis distances followed by permutation tests using Procrustes distance to assign statistical significance to pairwise comparisons of mean shape differences between groups. All graphs were made using R version 4.1.1 (R Core Team, 2022).

## 3 | RESULTS

### 3.1 | Overview of the early development of Malawi cichlids

To provide a visual guide assisting embryo staging for further analyses, we present an overview of development from fertilization until early juvenile stages, focusing on the formation of the major features of the external morphology. The consistent staging nomenclature (Supporting Information: Table S1) used throughout this study makes it the first comparative analysis of the entire embryogenesis across multiple closely related, yet morphologically distinct cichlid species. Furthermore, we include two populations of AC ("Salima" and "Mbaka") and highlight instances of visible intraspecific variation between the two.

Overall, the development of the examined species closely resembles descriptions for other African cichlids (de Jong et al., 2009; Fujimura & Okada, 2007; Morrison et al., 2001; Otten, 1981; Saemi-Komsari et al., 2018; Woltering et al., 2018). As such, and unlike zebrafish or medaka, these cichlids have large and yolk-rich eggs, supplying essential nutrients for the developing embryo until it transforms into an actively feeding juvenile (Figure 1e). The eggs are surrounded by a translucent

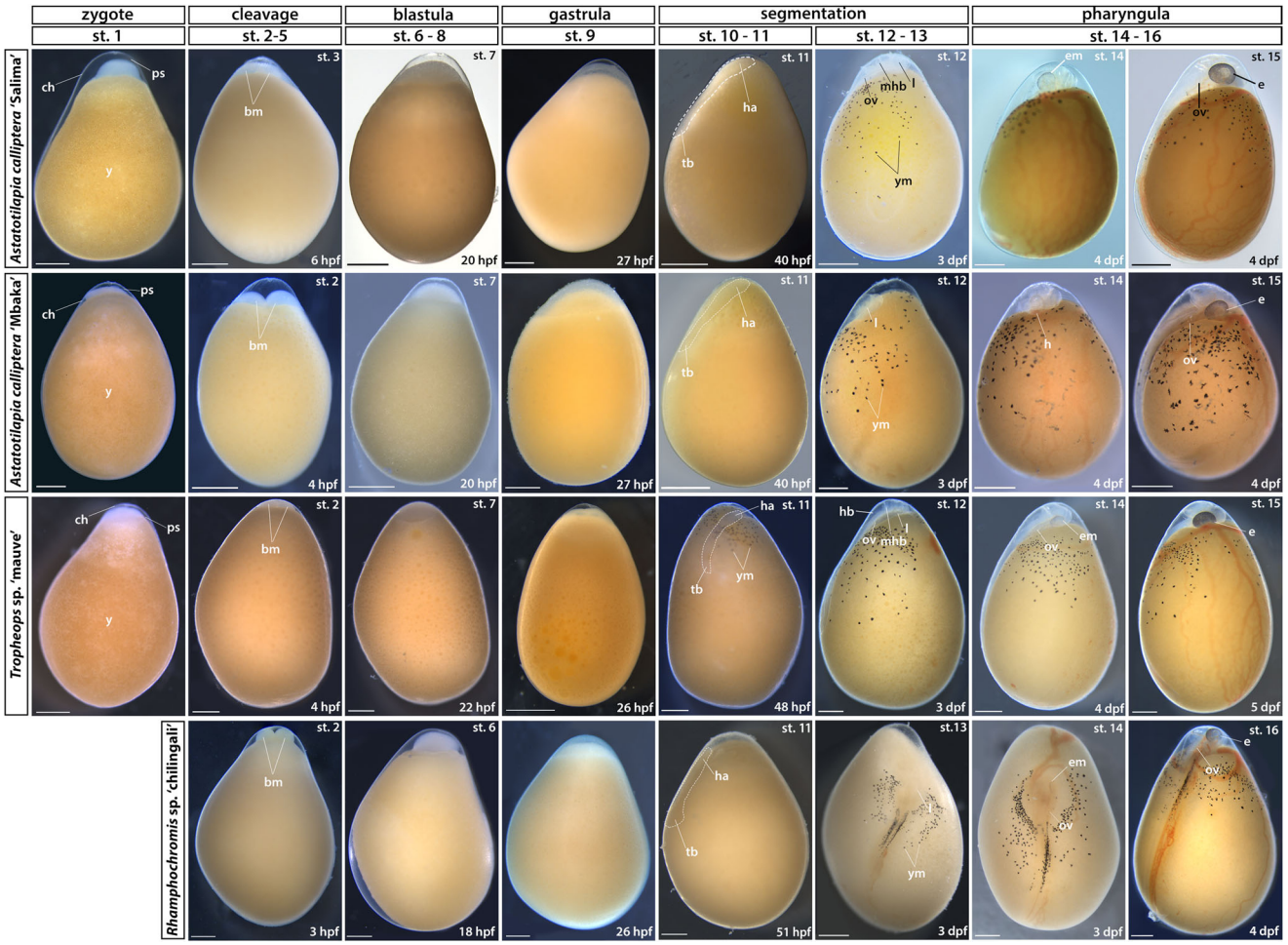


FIGURE 2 Early embryonic development (zygote to pharyngula). Stage numbering following the staging table of *Oreochromis niloticus* (Fujimura & Okada, 2007) (see Supporting Information: Table S1 for stage descriptions and associated developmental landmarks). Embryos undergoing somitogenesis are outlined in the "segmentation" stage. Lateral views except for dorsal views in RC st. 12–16. No st. 1 (zygote) image available for RC due to their prolonged courting and breeding behavior. bm, blastomeres; ch, chorion; dpf, days postfertilization; e, eye; em, eye melanophores; ha, head anlagen; hb, hindbrain; l, lens; mhb, midbrain-hindbrain boundary; ov, otic vesicle; ps, perivitelline space; st, stage; tb, tailbud; y, yolk; ym, yolk melanophores. Scale bar = 1 mm.

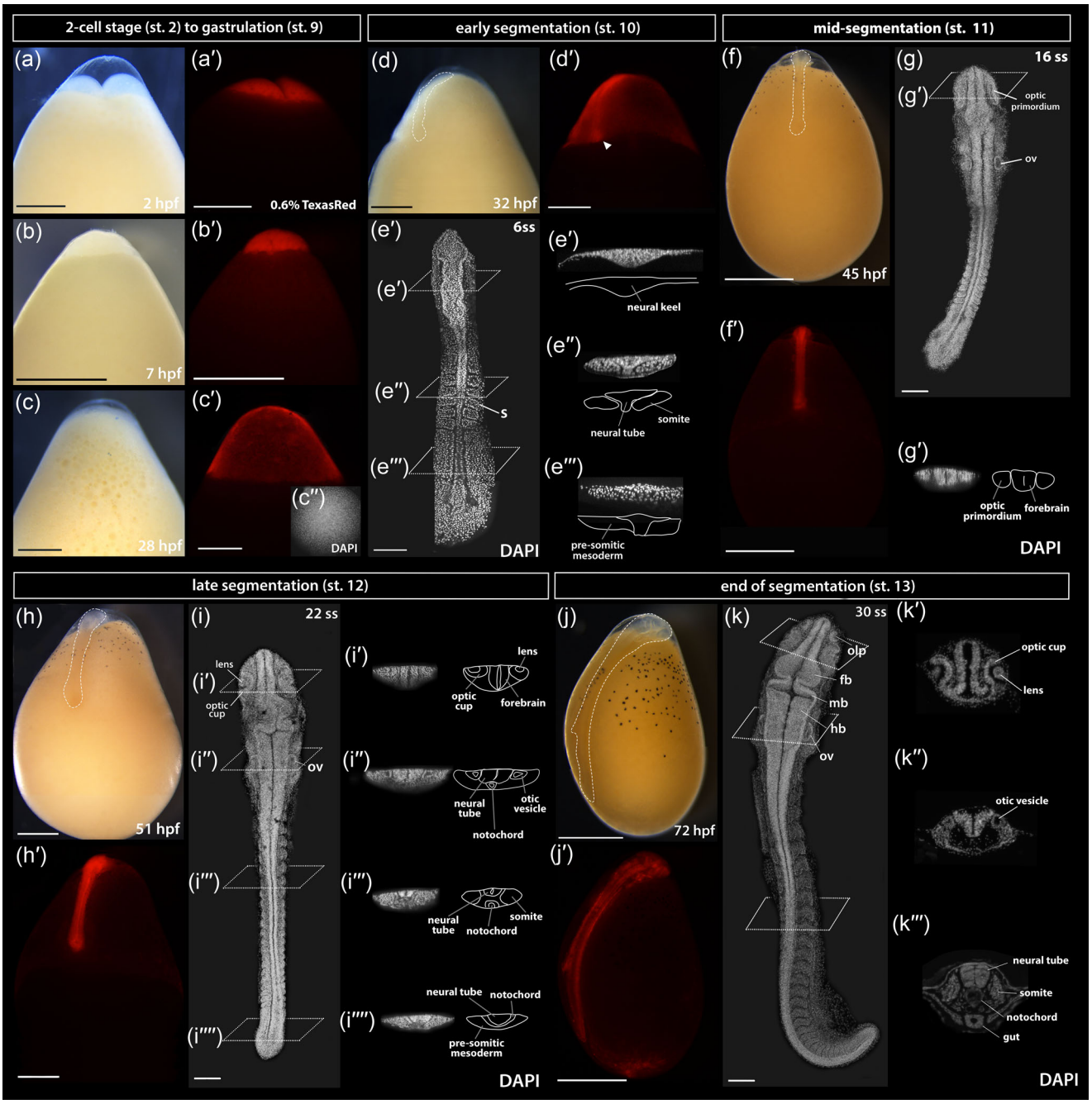


**FIGURE 3** The development of *Astatotilapia calliptera* embryo from two-cell stage until pharyngula. To observe morphology of live embryos, the fluorescent TexasRed dye was injected at the single-cell stage and it remained detectable in the tissues until at least 3 dpf (pharyngula stage). All whole-mount images (a–d′; f–f′; h–h′; and j–j′) are lateral views with the animal pole facing up and the vegetal pole facing down. The same embryo is shown across the series in both brightfield and under RFP fluorescence conditions except for the two-cell stage (a–a′), for which an uninjected control embryo is shown in brightfield (a). The embryos in (e), (g), (i), and (k) were dissected from yolk, stained with DAPI to visualize nuclei and imaged from the dorsal side with the anterior end of the embryo facing up. The specimen in c″ was stained with DAPI following the removal of the chorion, here shown in the view from the animal pole. Optical sections in all except for 28ss where histological sections are presented. Dashed lines in (d), (f), (h), and (j) show embryo outlines. The timing of development is given in hours postfertilization (hpf) at 27°C. DAPI, 4′,6-diamidino-2-phenylindole; fb, forebrain; hb, hindbrain; l, lens; mb, midbrain; oc, optic cup; olp, olfactory placode; op, optic primordium; ov, otic vesicle, ss, somite stage. Scale bar in a–d′; f–f′; h–h′; and j–j′ = 1 mm; 100 μm in all others.

chorion and the embryo develops on top an opaque yolk (ch and y in Figure 2, st. 1).

### 3.1.1 | Embryonic development from zygote to gastrula

On the first day postfertilization (dpf), the embryos undergo meroblastic cleavage divisions and enter the blastula period. The first mitotic division occurs within 2.5 h postfertilisation (hpf) and each following one is paced at 2–3 h (Figure 2, st. 2–5). The blastomere (bm in Figure 2, st. 2–5) arrangement resembles that of zebrafish, with regular grids of $2\times2$, $2\times4$, $4\times4$, and $4\times8$ forming on the animal pole of the egg. By the 64-cell stage, the individual blastomeres are difficult to distinguish and the regularity of cell arrangement is no longer discernible. Over the next few hours, the cells start to form a ball-shaped blastodisc located on the animal pole of the egg which subsequently flattens as embryo progresses from blastula (Figure 2, st. 6–8) to gastrula (Figure 2, st. 9). The incremental flattening of blastodisc transforms it into a uniformly thick layer—the blastoderm—which begins to cover the yolk from the animal pole in the process of epiboly (Figure 2, st. 9–11).

### 3.1.2 | Development from gastrulation through somitogenesis

From the onset of gastrulation (Figure 2, st. 9) until midsomitogenesis (Figure 2, segmentation, st. 10–12), the embryo proper becomes difficult to distinguish from the surrounding extraembryonic tissues and its features are not easily observable in live embryos (Figure 2, st. 9–12). Consequently, we examined these stages more closely using fluorescent dye microinjections of single-cell embryos with TexasRed and nuclear DAPI staining of dissected and fixed embryos (Figures 3 and 4). The period of somitogenesis (i.e., process of sequential addition of mesodermal somites) was of particular interest due to its temporal concurrence with specification and migration of the NCCs. We determined the chronology of gastrulation and somitogenesis and the total number of generated somites in each species, since the somite stage (ss) is a commonly used index to stage-match embryos. Due to its established experimental amenability (Clark et al., 2022), we used AC embryos to illustrate the common features of cichlid development as observed in live specimens (Figure 3).

Following cleavage and blastula stages (Figure 3a,b, respectively), all species reach 20% epiboly around 26–28 hpf (Figure 2, st. 9, Figure3c). By 28–30 hpf (25%–30% epiboly), the cell density in the blastoderm is no longer uniform, with a more densely occupied region at one side of the blastoderm, marking the future embryonic axis (Figure 3d–d′). The embryo undergoes gastrulation, a process which results in three germ layers. Similarly to other cichlids (de Jong et al., 2009; Kratochwil et al., 2015; Woltering et al., 2018) but unlike zebrafish (Kimmel et al., 1995), embryos start segmenting before epiboly is complete (Figure 2, st. 10–13; Figure 3d,e).

By 32 hpf in AC (Figure 2d, st. 10, 4–6 ss; Figure 3e), the embryonic axis is discernible by eye and the posterior end of the embryo (Figure 3e‴) is flatter and wider (plate-like) compared with the anterior end. At this point, although the first few somite pairs have already formed (Figure 3e,e″), the embryo still thins down to a single cell layer (epidermis) at the extreme margins where it joins the rest of the blastoderm spreading over the yolk, as visible in the optical transverse sections at the prospective head region (Figure 3e′). At this early stage in somitogenesis, the region located anterior to the first somites has the characteristic triangular shape of the neural keel (Figure 3e′), a structure formed from neural plate and a precursor of the neural tube in teleosts (Lowery & Sive, 2004).

Over the next 24 h, the embryos thicken and elongate via sequential addition of somites. The unsegmented tail region has a bud-like appearance (Figure 3f–i) and progressively shrinks as the somitogenesis progresses. The development of optic, otic and olfactory vesicles (precursors of the eye, ear, and the olfactory epithelium, respectively) occurs alongside body axis elongation (Figure 2, st. 12–13; Figure 3f–k; Figure 4d–f). Specifically, around 8–9ss (Figure 4b), the optic primordia begin to form from the anterior neural keel, whereas the otic vesicles located beside the caudal region of the hindbrain become discernible by 12ss (Figures 3g and 4c). The first visible pigmentation—black melanophores—appears on the yolk along the midsection of the elongating embryo and soon after spread over the yolk (Figure 2, st. 10–11 for TM, st. 12–13 for AC and RC). The lenses in the optic cups are clearly visible by 18ss in all species (Figures 3i and 4d). The brain grows and undergoes regionalization during the second half of the segmentation period (Figure 2, st. 12–13; Figure 3f–k; Figure 4c–f). The midbrain–hindbrain boundary (the isthmus) of the developing brain becomes prominent around 22–23ss (Figure 2, st. 12–13; Figure 4e). The olfactory placodes and three brain vesicles (forebrain, midbrain, and hindbrain) become apparent by 30ss (Figures 3k and 4f). Concurrently with the late phase of somitogenesis (>28ss), epiboly approaches 90% (i.e., the posterior end of the embryo reaches the vegetal pole of the egg) and trunk somites become V-shaped


**FIGURE 4** Embryo morphology throughout the segmentation period (st. 10–13). (a–f) Development of anatomical landmarks is correlated with progression of somitogenesis in all examined species, that is, somite stage is a good predictor of embryo morphology. (g) Embryos dissected at the end of their segmentation exhibit differences in the total somite number. All embryos were dissected from yolk, stained with DAPI to visualize nuclei, and imaged from the dorsal side with anterior–posterior orientation as indicated on A for (a–f) and in (g). A, anterior; mhb, midbrain-hindbrain boundary; olp, olfactory placode; P, posterior; ss, somite stage; st, stage. Scale bar = 100 μm.

(Figures 3j–k and 4f). At this point, the beat of the transparent heart is visible in embryos dissected from yolk (data not shown).

Although the overt processes of embryogenesis occurring until the end of the segmentation period seems to be generally conserved between the examined species, we observed divergence in the total number of generated somites and the total embryo size (Supporting Information: Figure S3). Specifically, AC has 30–32 somites, TM 34, whereas RC up to 38 (Figure 4g). Despite this key difference, the developmental progression in these species, marked by the gradual acquisition of anatomical landmarks such as the optic and otic vesicles, seems to be more tightly correlated to the number of already formed somites (i.e., ss) than to the relative completion of somitogenesis (the ratio of existing somites to the total number per species). Moreover, except for the addition of new somites and increase in size, which was positively correlated to increasing somite number (Supporting Information: Figure S3), we did not observe any further changes to external morphology of both RC and TM past 30ss (i.e., the end of segmentation in AC) when compared with AC (Figure 4g). Altogether, our results show the embryo morphology at a given ss is largely matched between species throughout the segmentation period, irrespective of the variation in the overall number of produced somites.

### 3.1.3 | Development during the pharyngula period

The pharyngula period (st. 14–16) is characterized by the progressive development of dark eye coloration, an increasing vasculature on the yolk surface and circulation of red blood cells. The pigmentation of retinal epithelium starts at st. 14 (Figure 2) and increases in intensity until the hatching period (Figure 5, st. 17–18) when the eyes become fully opaque. The somites located posterior to the trunk region gradually change from a rounded rectangular shape to V-shaped (Figure 4g) as they differentiate into myotomes (myo in Figure 5, st. 17) in an anterior-to-posterior order. The embryo now extends around the entire length of the yolk with the tail curling inside the chorion (Figure 2, st. 16). The head thickens and becomes bulbous with the development of the brain and elements of the face (Figure 2 st. 16, Figure 3j).

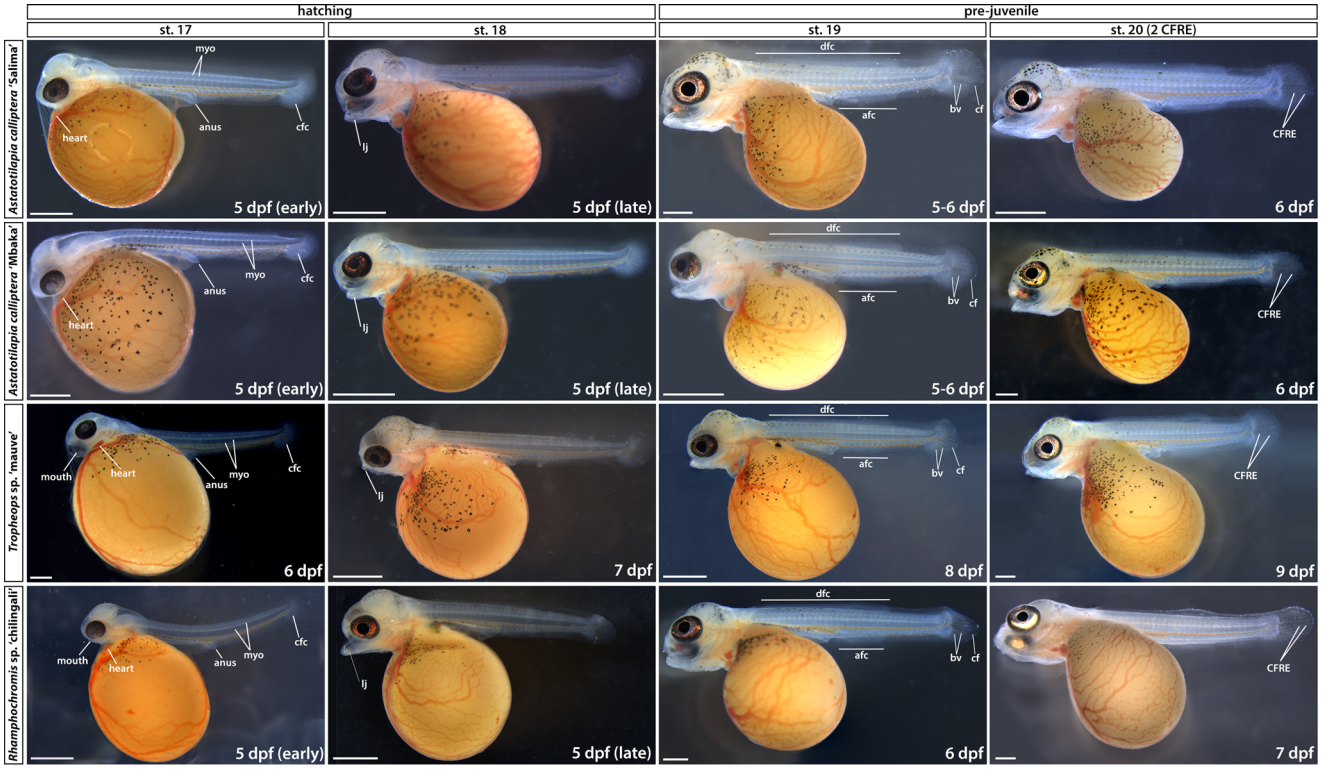


FIGURE 5 Late embryonic development to early prejuvenile stages (hatching to stage 20). Stage numbering following the staging table of *Oreochromis niloticus* (Fujimura & Okada, 2007) (see Supporting Information: Table S1 for stage descriptions). afc, anal fin condensation; bv, blood vessels; cf, caudal fin; cfc, caudal fin condensation; CFRE, caudal fin ray elements; dfc, dorsal fin condensation; dpf, days postfertilization; myo, myomeres; st, stage. Scale bar = 1 mm.

### 3.1.4 | Development from hatching (st. 17) to st. 20: Early stages of development of skin pigmentation and skeletal system

Hatching period encompasses the transition from pharyngula (a late embryonic stage) to postembryonic (or prejuvenile) stages of development and marks the onset of a gradual formation of adult traits including the head cartilaginous skeleton and body pigmentation (Figure 5, st. 17–18). As with other direct-developing species (Jones, 1972; Balon, 1977, 1999; Woltering et al., 2018) the adult body plan, including the anal and dorsal fins, is progressively attained throughout the postembryonic stages (Figures 5–7). Stages 17–19 (Figure 5) were delimited based on the head morphology (Supporting Information: Table S1), whereas from st. 20 onwards, the number of caudal fin ray elements (CFRE) was used as a diagnostic feature. At st. 17, the ventral side of the head is attached to the yolk but a small opening, marking future mouth, can be distinguished just above the heart (Figure 5). The tail is separated from the yolk sac. Despite some intra- and interclutch variability, most embryos hatch at this stage (5 dpf for AC and RC, 6 dpf for TM). At st. 18 (Figure 5), the head lifts from the yolk, the mouth opens and occasional movements ("wiggles") of the tail are observed. At the following stage (Figure 5, st. 19), both the operculum covering the gills and the lower jaw begin to move sporadically and the mesenchymal condensations marking future anal and dorsal fin develop (afc and dfc in Figure 5, respectively). The developing blood vessels in the caudal fin (bv and cf in Figure 5) become more prominent. Embryos at st. 20 (Figure 5) have fully functional and rapidly moving oral jaws and two CFRE. This stage marks the transition from embryonic to prejuvenile stages when the adult body plan and external morphology will be gradually acquired.

### 3.1.5 | Development from st. 21 to complete body wall closure (st. 27–28): Continued formation of species-specific phenotypes

The embryos start to right themselves and soon can swim upright. From st. 21, the caudal, dorsal, and anal fins develop pigmentation, starting with melanophores (mel in Figure 6, st. 21). Differences in the head and jaw morphology, body shape and pigmentation patterns between species are increasingly noticeable. For instance, at st. 23 (Figure 6), the melanophore flank pigmentation remains scarce in TM, AC "Mbaka" has irregular melanic patches (mp, Figure 6, st. 23) spread out over its flanks, whereas in RC, melanophores form a specific pattern of large, oval clusters distributed on the flanks along the midline and dorsum. Notably, the melanophore distribution is considerably more uniform across the flank in AC "Salima" compared with its co-specific "Mbaka".

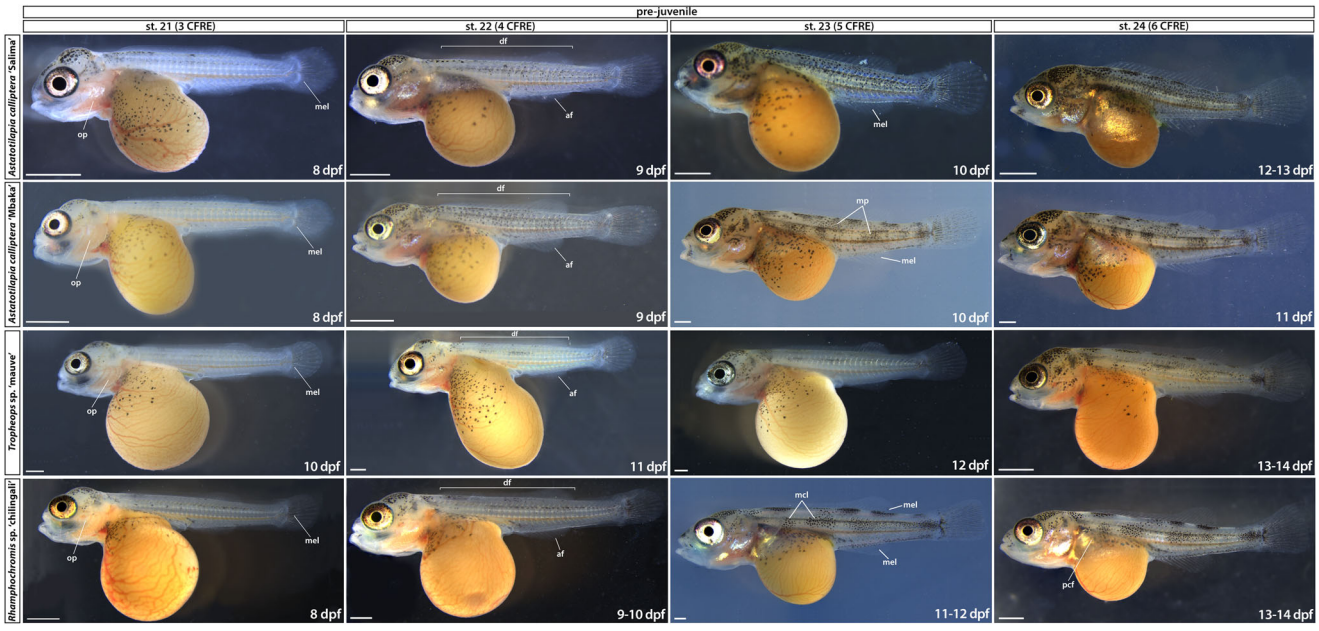


**FIGURE 6** Prejuvenile development (stages 21–24). Stages are delimited based on the number of CFRE. Time ranges (in days postfertilization) given to indicate the duration of the corresponding stage. af, anal fin; CFRE, caudal fin ray elements; df, dorsal fin; dpf, days postfertilization; mcl, melanophore clusters; mel, melanophore; mp, melanic patches; op, operculum; pcf, pectoral fin; pvf, pelvic fin; st, stage. Scale bar = 1 mm.

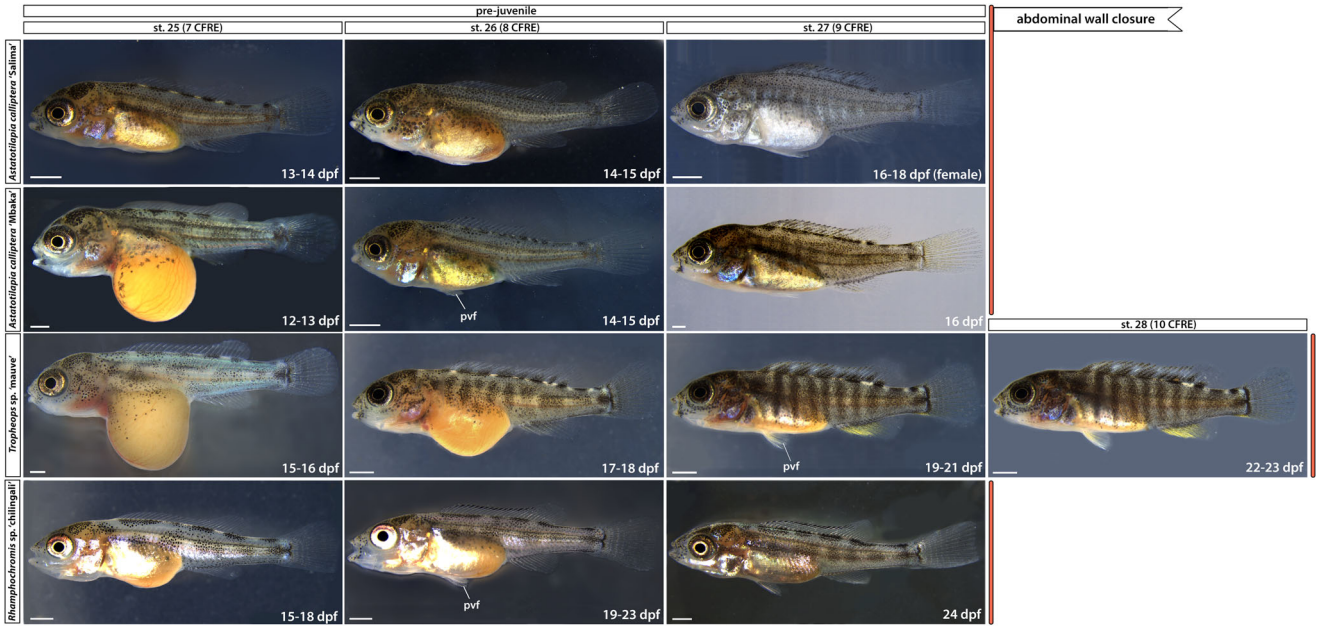


**FIGURE 7** Late prejuvenile development (stage 25 to abdominal wall closure). Time ranges (in days postfertilization) given to indicate the duration of the corresponding stage. Note the silvery hue of *Astatotilapia calliptera* "Salima" female at st. 27 compared with a darker male fish shown for st. 26. dpf, days postfertilization; pvf, pelvic fin; st, stage. Scale bar = 1 mm.

At the same stage, the interspecific differences in body shape and head morphology are also apparent (Figure 6, st. 23). For example, the body of RC is more elongated along the anterior–posterior axis compared with shorter and more corpulent bodies of TM and AC. The pelvic fins form by st. 26 in all species except TM, in which they appear at st. 27 (pvf in Figure 7). Interestingly, the closure of the abdominal wall over the yolk sac, marking the onset of the juvenile period and thus the end of our staging table, is similarly delayed by one stage in TM compared with AC and RC (Figure 7, st. 27–28). These two instances exemplify heterochrony in the development of morphological features where particular characters do not always appear simultaneously or in the same order between species. At this point, the yolk is fully absorbed into the body cavity and juvenile fish start to feed actively.

Overall, the overview of the early development of Malawi cichlids presented here is a clear illustration of the wide range of biological diversity harbored both between and within species. Based on the readily visible external features alone, the embryonic development of examined cichlids is very similar until hatching (Figures 2 and 4), followed by a rapid appearance of species-specific morphologies (Figures 5–7). Despite these broad similarities in the early ontogeny, the examined species exhibited considerable variation in the timing or rate of development, including during the segmentation period and posthatching stages.

## 3.2 | Pervasive heterochrony during cichlid embryogenesis

### 3.2.1 | Duration of somitogenesis is similar between species despite variation in rates (st. 10–13)

The temporal periodicity of somite addition, termed the segmentation clock, is known to exhibit vast species-specific variation in the pace of its progression (Hubaud & Pourquié, 2014). Considering the differences in the total numbers of formed somites between species (30–32 in AC, 34 in TM, and 38 in RC, Figure 4g), we tested for variation in segmentation rates. To collect a representative sample, we aimed to sample 2–3 embryos from the same clutch ($n = 3$) at each given time point. However, due to TM's small clutch size, we were unable to follow its development in a similarly detailed manner (Supporting Information: Table S2).

The rates of somitogenesis were inferred relative to the onset of segmentation, coinciding with the end of gastrulation and appearance of neural keel in the anterior region, to minimize the temporal variation introduced by the use of chronological time (i.e., hpf) to stage embryos of different species. Despite frequent sampling, we were unable to identify embryos with less than four somites, suggesting that these form almost simultaneously in both AC and RC. We did not observe any pronounced variation among sampled specimens of

the same species and the slight differences among RC embryos could be explained by the extended duration of their mating behavior (2–3 h) compared with AC (0.5–1 h). Overall, the segmentation rates of both species follow linear trends with slightly, albeit statistically significant, differing slopes (one-way analysis of variance, $F(1, 83) = 4.414$, $p = .039$) and the total duration of somitogenesis is similar between them, lasting about 35 h (Figure 8a). Considering the difference in the total number of somites generated by each species (38 in RC and 30 in AC), the segmentation seems to progress at a faster pace in RC early in the process (i.e., during formation of the first few somites) compared with AC. This is supported by the significant differences between species in y-intercepts of the inferred segmentation rates ($F(3, 83) = 863.5$, $p < .001$).

The appearance of morphological structures, such as otic vesicles, is tightly correlated with absolute somite number in both species (e.g., at 30ss, AC and RC embryos have the same anatomical structures). Thus, past this point, RC appears to only elongate further without the addition of further anatomical structures. Consequently, since segmentation is progressing faster in RC than AC, these anatomies also develop faster in RC and only additional somites form in the remaining time during somitogenesis. These heterochronic shifts explain how the overall duration of segmentation is conserved between species with different somite numbers.

### 3.2.2 | Posthatching development (st. 16–28) exhibits intra- and interspecific temporal variability

Since interspecific temporal differences were observed also throughout the posthatching stages (Figures 5–7), we quantified this variation by following embryos across their development and contrasting their developmental trajectories against chronological time elapsed since the day of fertilization (Figure 8b). Our results indicate that the development of each of the species follows a slightly distinct temporal path with overlaps at specific stages. For example, the developmental trajectory of AC "Mbaka" diverges around st. 18 from the other species and remains separate except for a brief overlap with RC at st. 20–22. The former develops the fastest among the species, progressing between consecutive stages within a day to reach the last embryonic stage (st. 27) at 16 dpf. Contrarily, RC embryos tend to be the slowest (st. 27 at 23–24 dpf). Although there is one more stage (st. 28) in TM's trajectory, they still enter the juvenile period ahead of RC (21–23 dpf, Figures 7 and 8b). Interestingly, the

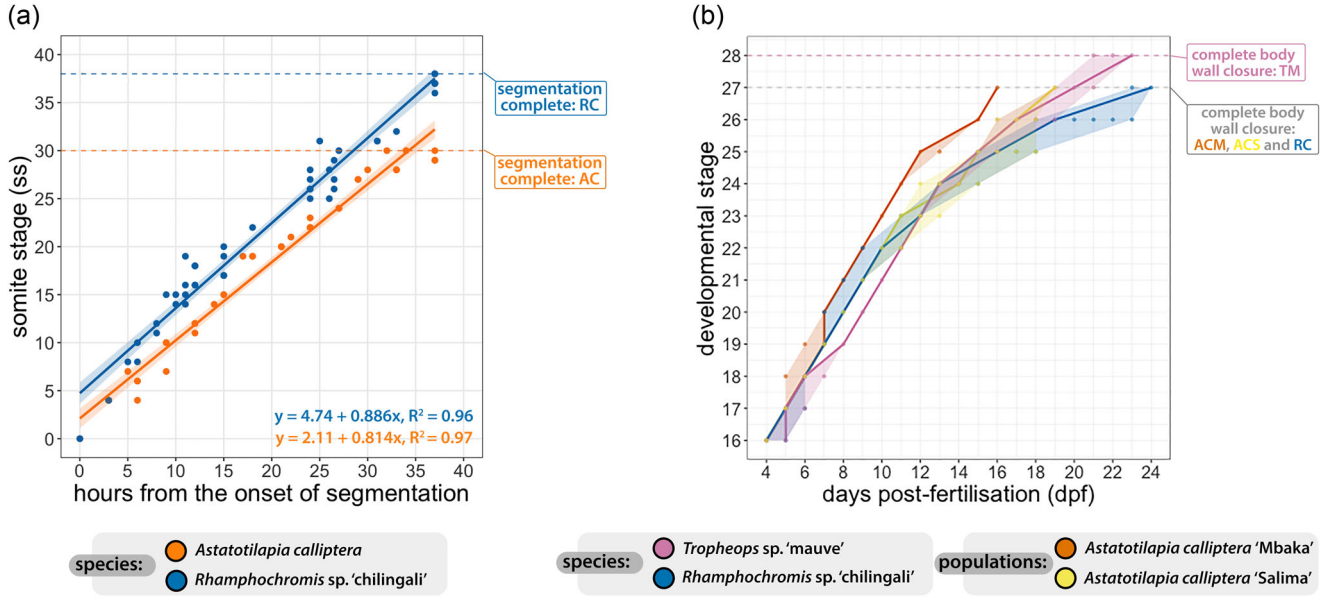


FIGURE 8 Timelines of cichlid development during segmentation (st. 10–13) and developmental trajectories from hatching (st. 16) until complete abdominal wall closure (st. 27/28). (a) Somite stage (ss) against hours elapsed from the onset of segmentation. Solid lines correspond to linear regressions representing idealized rates of somitogenesis, whereas shaded bands present associated 95% confidence intervals. (b) Time ranges of the posthatching stages (st. 16–28). The solid trend line corresponds to median values and shaded bands encompass all individual trajectories of the embryos followed through development at 27°C. At least three animals from three different clutches were inspected at each time point. Although all raw data points are presented on both panels, in some instances they are occluded due to the overlap between them. AC, *Astatotilapia calliptera*; ACM, *Astatotilapia calliptera* "Mbaka"; ACS, *Astatotilapia calliptera* "Salima"; RC, *Rhamphochromis* sp. "chilingali"; TM, *Tropheops* sp. 'mauve.'

timing and duration of some stages demonstrate intra- and interspecific variation, particularly in the later phase of the prejuvenile development (represented by the width of the shaded regions in Figure 8b, st. 22–28). Among the examined species, the embryos of AC "Mbaka" exhibit the least temporal variability, whereas RC embryos vary the most. These findings add further evidence that the developmental trajectories of these cichlids, especially in the temporal aspect, seem to be already distinct at the time of embryogenesis. The considerable variation in timings between species highlights the potential risks associated with relying solely on embryo age or morphological landmarks to guide comparative studies in this clade.

## 3.3 | The early ontogenies of skeletal system and body pigmentation

To determine when differences in cichlid NC-derived trait development are first evident, we investigated the early formation of the craniofacial skeleton and skin pigmentation. The overt development of these traits begins around the time of hatching (Figure 5, st. 17–18) and continues throughout the postembryonic period (Figures 6 and 7).

### 3.3.1 | Divergence in craniofacial shape is evident at the onset of cartilage deposition

We investigated the formation of craniofacial cartilages (Figure 9) to assess for qualitative and quantitative differences between species across early ontogeny (Supporting Information: Figure S2 and Table S3). The first cartilaginous element of the pharyngeal skeleton—primordial ethmoid plate—begins to form at st. 17 (5 dpf in all species, ep in Figure 9). At st. 18 (5–6 dpf in AC and RC, 7 dpf in TM), in addition to the formation of almost all the cartilaginous structures of the lower jaw (except for the basihyal), the palatoquadrate of the upper jaw is also present (pq in Figure 9). The branchial arch elements, although formed in AC and RC, are not detected at this stage in TM (ba in Figure 9, st. 18). By st. 19 (6–7 dpf in AC and RC, 8 dpf in TM), chondrogenic condensations of the occipital arch appear around the eye orbit and the vomerine process, the epiphyseal bar and the branchiostegal rays have formed. The articular process of the Meckel's cartilage and basihyal form in the jaw and the branchial arches are now fully developed in TM (ba in Figure 9, st. 19). At st. 20 (7–8 dpf in AC, 7 dpf in RC, and 9 dpf in TM), the upper lip (black arrowheads, Figure 9) is present. The consistent temporal shift in the development of the craniofacial complex by at least 1 day in TM compared with AC and RC (Figure 9) shows that timing differences are correlated with interspecific differences, further suggesting that heterochronies contribute to species divergence.

To quantitatively compare divergence in craniofacial development between species, we conducted geometric morphometric analyses on the lateral and ventral views of specimens stained for cartilage taken for st. 18–20 (Figure 10, Supporting Information: Figures S2, S4, and S5, and Tables S3 and S4). We used CVA to assess how well sample groups (here defined by species, stages, and a combination of the two) can be differentiated from one another by maximizing the between-group to within-group variance ratio. In the lateral aspect (Figure 10a), the primary axis of variation (CV1, 64% of total variation) described differences in the craniofacial slope and separated samples by developmental age, with the greatest variation between st. 18 and the following stages (st. 19–20) in both AC and RC (Procrustes distance = 0.1865, $p < .001$ for AC st. 18 vs. AC st. 19; Procrustes distance = 0.1727, $p < .001$ for RC st. 18 vs. RC st.19, Supporting Information: Table S4). This suggests a large change to craniofacial shape early in ontogeny in these species compared with a more gradual development in TM (Procrustes distance = 0.0834, $p < .05$ for TM st. 18 vs. TM st. 19). At st. 19 and 20, the variation between and within species was smaller, albeit statistically significant ($p < .05$) for all pairwise comparisons except for TM and RC at st. 19 (Procrustes distance = 0.0576, $p = .0608$). Overall, the development of the lateral aspect of the craniofacial complex in these species followed similar but distinct trajectories.

Akin to lateral development, CVA for the ventral aspect (Figure 10b) also separated samples along the ontogeny (CV1, 61% of total variation) and described the width of the ventral aspect. The differences between groups, although small, were statistically significant across all pairwise comparisons ($p < .05$, Supporting Information: Table S4), indicating early onset of a lasting divergence between species. Of note, the greatest variation within species between consecutive stages was observed in AC between st. 18 and st. 19 (Procrustes distance = 0.2112, $p < .001$), similarly to the trend observed in the lateral aspect, suggesting a more pronounced remodeling of the craniofacial shape occurring in early development in this species than in TM and RC. Moreover, the differences between AC and the other two species at st. 20 were small (Procrustes distances < 0.065 in pairwise comparisons, $p < .001$), supporting the position of AC's craniofacial phenotype as an intermediate between more specialized morphologies of RC and TM. Altogether, our results demonstrate that despite

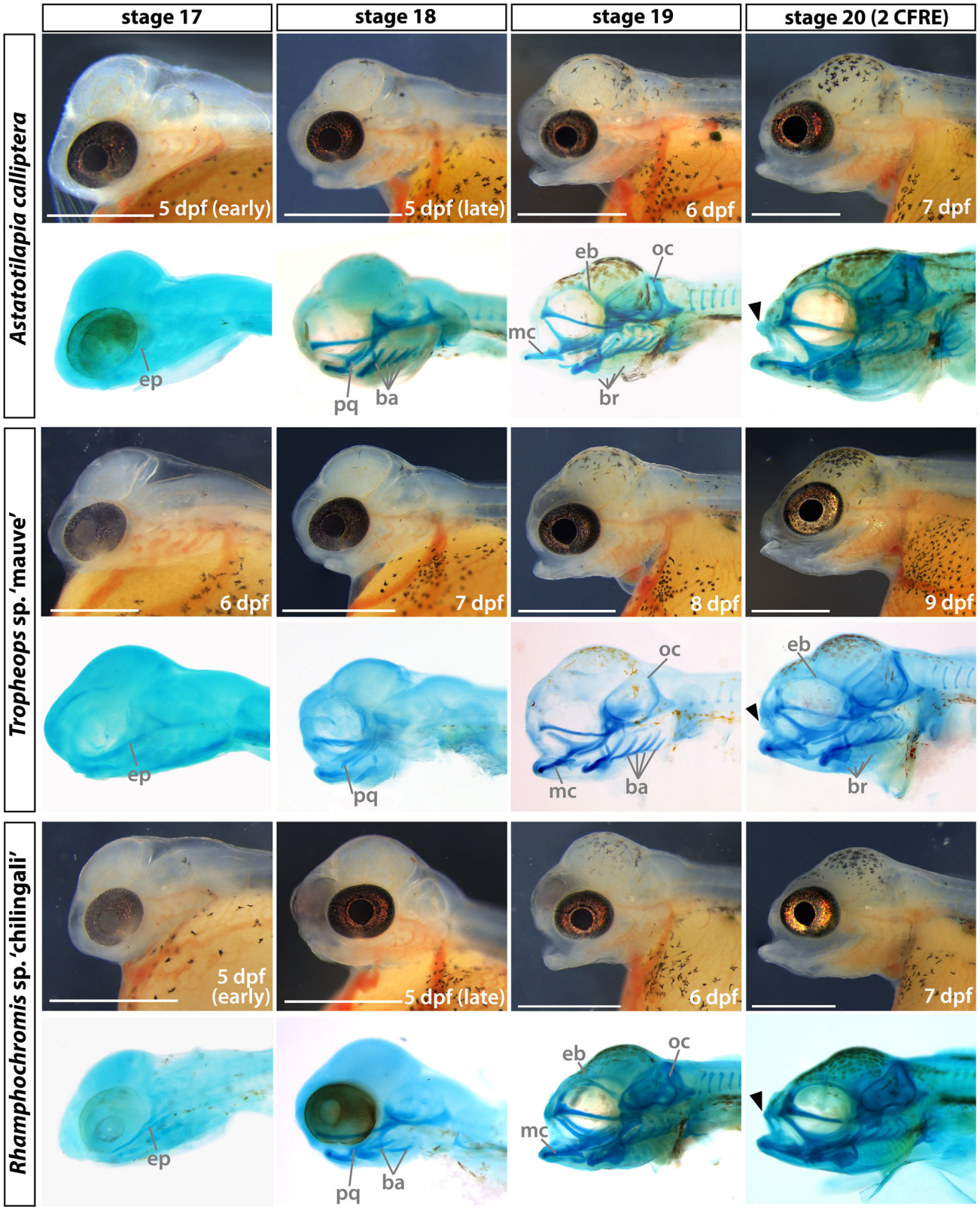


FIGURE 9 Development of the craniofacial morphology of *Astatotilapia calliptera, Tropheops* sp. 'mauve,' and *Rhamphochromis* sp. 'chilingali' embryos. All images are left lateral views, dorsal side toward the top, and rostral side to the left. For each species in turn, panels in the bottom rows present cartilage stains of stage-matched specimens to those depicted in brightfield (top rows). Due to the lack of perceivable differences between AC 'Salima' and 'Mbaka,' only the latter is shown. ba, branchial arches; br, branchiostegal rays; CFRE, caudal fin ray elements; eb, epiphyseal bar; ep, ethmoid plate; mc, Meckel's cartilage; oc, occipital arch; pq, palatoquadrate. Scale bar = 1 mm.

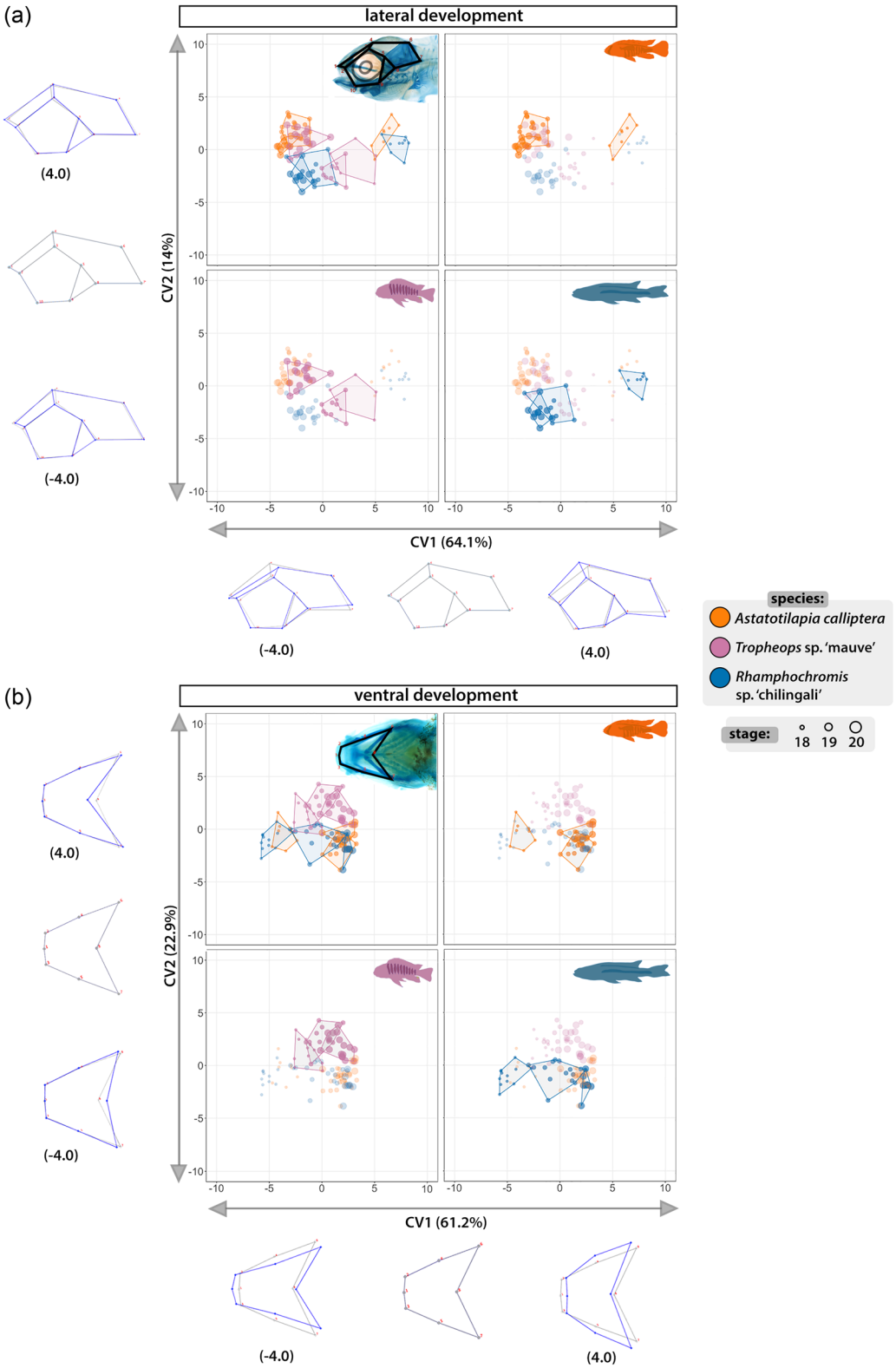


**FIGURE 10** Developmental trajectories of lateral and ventral craniofacial aspects are species-specific. Canonical variate analysis (CVA) through ontogeny shows significant differences in mean shape between species at most stages of development of craniofacial cartilages. Results from CVA of the lateral (a) and ventral (b) development with corresponding spectra of shape changes along the axes of greatest variation (CV1 and CV2). Colored polygons encompass all data points for each group composed of specimens of a given species at a specific stage. Developmental stages are indicated by the size of the point. All four panels in (a) and (b) present the same scatter plot with data points for different species highlighted in turn (clockwise from top left: all groups, *Astatotilapia calliptera*, *Rhamphochromis* sp. 'chilingali' and *Tropheops* sp. 'mauve'). The wireframes present the projected shape change along associated CV axis with gray frame corresponding to the overall average shape and blue frames representing the shape change along the spectrum of CV values from −4.0 to 4.0 along each axis.

initial external similarities, the craniofacial cartilages have species-specific morphologies from the onset of their development along distinct paths.

### 3.3.2 | Differences in head epidermal pigmentation are apparent as soon as the first pigment cells appear

To identify species-specific divergence in pigmentation development, we examined the timing of pigment cell appearance on the dorsal side of the head. The head epidermis is the first area to be populated by all three major cell types, appearing significantly earlier than the chromatophores underlying the flank pigment patterns. A summary schematic of the different cell populations and specific head regions described below is presented in Figure 11c.

The first black melanophores are detected at st. 16 (Figure 11a) in some embryos of AC "Salima" and TM but not in the other two species (Figure 11b). At st. 17 (Figure 11a), melanophores on the dorsal surface of the head and rostral trunk region are now present in all inspected individuals. In AC and TM, these are thin and elongated with several projections each, whereas the larger and wider ones are not fully pigmented. In contrast, melanophores observed in RC appear small and rounded, presumably due to the centralized localization of the dark pigment in the cell. Round reflective iridophores begin to aggregate in the posterior patch (blue arrowheads, Figure 11a,b) in all species but not across all examined embryos. By st. 18 (Figure 11a), more pigment cells have appeared on the dorsal surface of the head in all species, including the first signs of yellow pigmentation in AC "Salima" and TM (yellow arrowheads, Figure 11a, st. 18; Figure 11b). Iridophores continue to accumulate in the skin covering the dorsal hindbrain. Isolated round iridophores are sparsely distributed among the melanophores on the head region in all species except for RC (white arrowheads, Figure 11a, st. 19; Figure 11b). Lastly, at st. 20, all three chromatophore types are present in all taxa (Figure 11a–c) and the melanophores on the dorsal head region tend to have a "snowflake-like" morphology, that is, with a small, circular center and multiple radially extending projections that make contact between neighboring cells. Intriguingly, some melanophores (as seen on AC "Mbaka" in Figure 11a, st. 20) do not fit this description and instead of long projections, have jagged edges and appear to cover a larger surface area than the former type. By now, single iridophores (white arrowheads, Figure 11a,c, st. 20) and xanthophores in the posterior region are also found in RC but the latter appear less conspicuous (or fainter) and numerous than in the other taxa. Another major difference in pigmentation at this stage concerns the abundance of iridophores in the posterior patch, that is, it is much more pronounced in AC "Salima" than in any other species (Figure 11a, st. 20). Generally, although the order of appearance of each chromatophore type (melanophores first, xanthophores last) and the stereotypical cell distributions at stage 20 (Figure 11c) showed a close resemblance between species, we observed intra- and interspecific variation in the morphology, localization, and abundance of the specific cell types relative to the chronological (dpf) and developmental age (stage).

Altogether, our results demonstrate that the initial gross similarities in external morphology present during pharyngula and early hatching periods (st. 14–17, Figures 2 and 5) progressively decrease with the gradual appearance of species-specific phenotypes, including the pigmentation patterns and craniofacial morphologies, as the animals progress into juvenile and adult stages. Considering that both of these phenotypes showed interspecific variation at the onset of their overt formation, we hypothesize that these differences begin to be specified beforehand, that is, during early embryonic development.

## 4 | DISCUSSION

A long-standing goal of evolutionary developmental biology is to understand the mechanisms underlying morphological diversification. Since a considerable proportion of the crucial morphogenetic processes occur during embryonic development, studying variation in the early ontogeny is key to understanding when and how divergent phenotypes form. The challenge in addressing these questions lies partly in the paucity of multispecies systems showing natural variation yet offering the experimental tractability for comparative embryology similar to the conventional models. Here, we took advantage of the Malawi cichlid system to compare early development across multiple closely related species harboring extensive divergence in adult phenotypes such as body coloration and craniofacial skeleton. These adaptively relevant yet easily observable morphological traits, both derived from the NC, offered us an unparalleled opportunity to explore the differences in embryonic processes in the context of adult phenotypic diversity.

Overall, the early development of the four Malawi cichlids presented here is characterized by many clade-generic features common to other teleosts (e.g., neurulation via cavitation of the neural keel) and, more

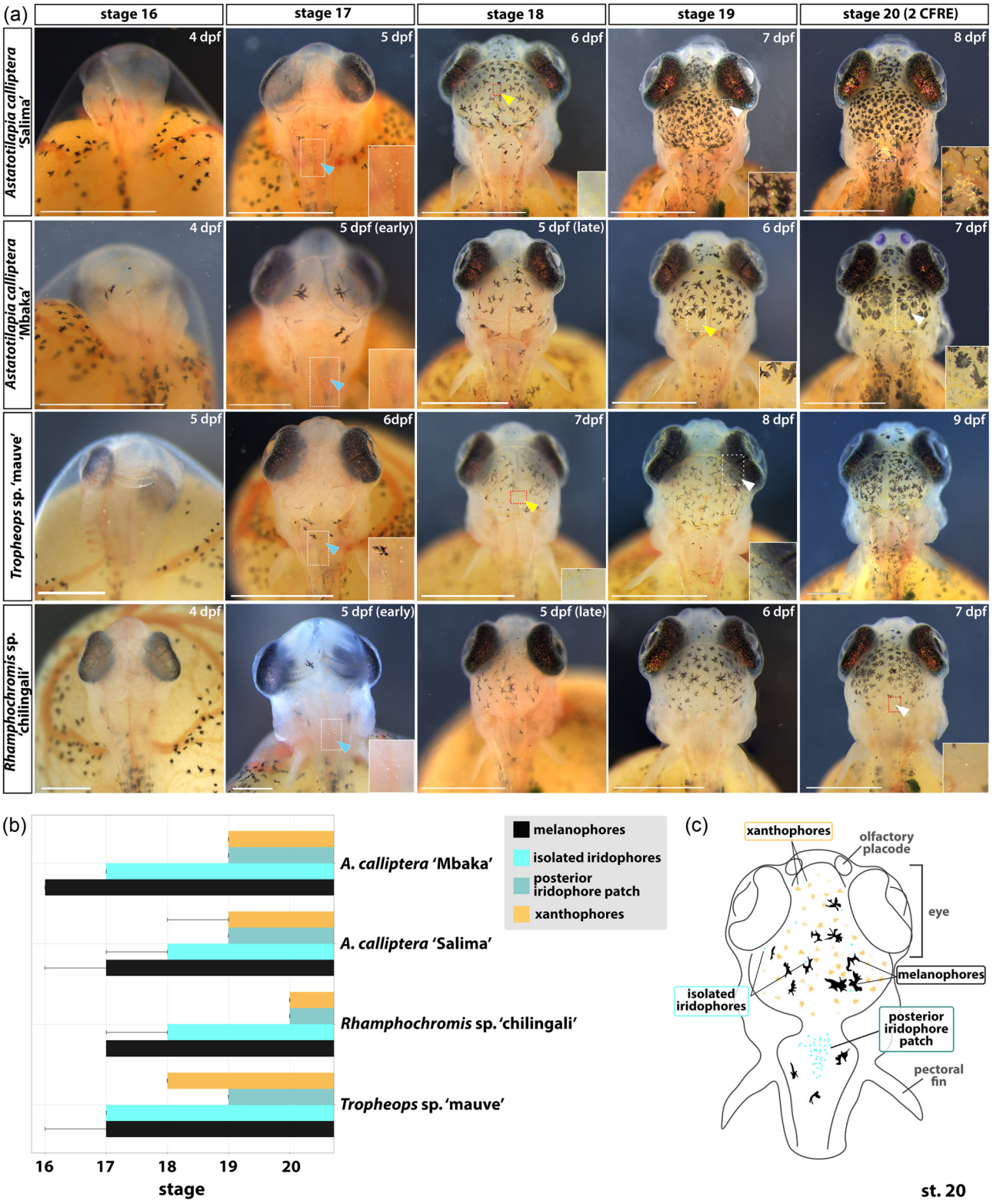


FIGURE 11 Development of skin pigmentation on the dorsal head region in *Astatotilapia calliptera* "Mbaka" and "Salima" *Rhamphochromis* sp. "chilingali" and *Tropheops* sp. 'mauve' embryos. (a) Developmental series of head pigmentation from the appearance of the first pigmented cells (st. 16, hatching) to the presence of all three pigment cell types in all studied species (st. 20). Insets show close-ups of the regions bounded by white rectangles. (b) Timeline of pigment cell appearance. Error bars indicate the earliest appearance of a given chromatophore type. Bar indicates presence in all examined specimens. The distinction of two iridophore subpopulations (i.e., "isolated" and "posterior patch") as highlighted in (c). (c) Schematic summary of the common features of the chromatophore distribution among cichlids in this study as observed at st. 20, viewed from the dorsal perspective. At least three animals from two different clutches were examined. Scale bar in A = 1 mm. CFRE, caudal fin ray elements; dpf, days postfertilization; st, stage.

specifically, other mouthbrooding cichlids, including the large maternal yolk supply and a direct development without a pronounced larval stage (Jones, 1972; Woltering et al., 2018). On the other hand, a careful comparison conducted in standardized conditions revealed a considerable degree of variability between these closely related species that contributes to their adult morphological diversity. This largely underexplored biological variation was primarily evident as anatomical and temporal (hetechronic) differences and was detected throughout early ontogeny, including the period of embryogenesis (e.g., somitogenesis) and post-hatching development (e.g., cartilage deposition and pigmentation development).

## 4.1 | Heterochronies are common in cichlid development

One of the most prevalent inter- and intraspecific differences concerned the variability in the timing, rate, and duration of specific developmental events. These included processes occurring in early embryonic development (i.e., segmentation) as well as later, throughout postembryonic stages (e.g., formation of the chondrocranium). Although heterochronies in early development have been reported among cichlids (Kratochwil et al., 2015), including both within and between clutches of the same species (Morrison et al., 2001), at least some of this variation could have been attributed to the effects of temperature on the speed of development in teleost fishes (Schröter et al., 2008). Our results show that these differences persist in controlled conditions. Consequently, heterochronies might render the use of chronological age in cross-species comparative work potentially confounding, thus we recommend the use of both the morphological staging and the time elapsed from fertilization in combination to infer developmental age and compare trait development and evolution.

The earliest and most striking differences were identified during somitogenesis, specifically in the number of generated somites in AC and RC, despite comparable total duration of the segmentation period. Intriguingly, the embryos did not visibly differ from one another in their progression of anatomical development when stage-matched by absolute somite number. Taken together, our results suggest that the modification of the somite "bauplan," which can be considered as about 30–32 somites, was two-fold. It involved (1) acceleration of the somite clock throughout segmentation and (2) the formation of the additional few somites at the very end of this period (i.e., an increase in the total number of cycles). Following these observations, we hypothesize that, due to its key roles in the development and patterning of the animal body, variability in this fundamental morphogenetic process of embryogenesis could have an important yet largely underexplored function in the evolution of cichlid phenotypic diversity. First, somites make broad contributions to the adult form, including the vertebral column and rib cage, cartilage and tendons, skeletal muscle and skin (Devoto et al., 2006; Holley, 2007; Morin-Kensicki et al., 2002; Stickney et al., 2000). The variation in the number of vertebrae has been previously described in the *Rhamphochromis* genus to range from 36 to 40 (Eccles & Trewavas, 1989), whereas *Astatotilapia burtoni* has 27 or 28 vertebrae (Woltering et al., 2018). Considering the relationship between the evolution of the skeletal system, including the vertebral column, and the body shape in the evolutionary history of vertebrates (Jones et al., 2018; Lindell, 1994; Müller et al., 2010; Richardson et al., 1998), it thus likely that divergence in the morphology of these derivatives contributes to the diversity of the body shapes across cichlid taxa (Malinsky et al., 2015). Second, the developmental dynamics of somitogenesis have been shown to influence the temporally coincident NC development, particularly in aspects such as the timing of delamination of NCCs from the neural tube and their subsequent migratory pathways (Loring & Erickson, 1987; Rocha et al., 2020; Sela-Donenfeld & Kalcheim, 2000; Teillet et al., 1987). Altogether, it is becoming clear that a good understanding of the processes of embryogenesis from comparative studies with wide taxon sampling will be required to elucidate its contribution to the developmental origins of morphological diversity of the clade.

## 4.2 | The species-specific phenotypes of NC-derived traits are determined early in ontogeny

The stunning diversity of cichlid body pigmentation patterns and craniofacial shapes renders them a perfect model to study the genetic and developmental basis of phenotypic trait diversification. Our results show that both NC-derived features have visibly species-specific morphologies from the earliest stages of overt development.

It is possible that observed temporal differences in chromatophore appearance are related to the different contributions of each cell type to adult phenotype, for instance, the earlier appearance of xanthophores in TM than in AC "Mbaka" and RC could be linked to the differences in the extents of underlying yellow pigmentation in the adult coloration. The variation in timing could be also related to cell–cell interactions between individual cell types and their environment (Patterson & Parichy, 2019), with temporal shifts in the appearance of

melanophores potentially influencing the subsequent emergence of xanthophores and iridophores. Further experimental work, including quantification of the chromatophore abundance, will be required to address these hypotheses.

Finally, the formation of body coloration in the examined head region did not seem to involve migration of mature, pigment-bearing cells but rather a sequential appearance of new chromatophores. This finding is in line with the account of color pattern formation in Lake Malawi cichlids *Dimidiochromis compressiceps* and *Copadichromis azureus* (Hendrick et al., 2019) but unlike zebrafish, where pigmented melanophores are known to exhibit migratory behavior, at least during stripe formation (Eom et al., 2012; Takahashi & Kondo, 2008). The species-specific trajectories of cichlid coloration could be thus set up before that, for instance, during migration of the undifferentiated pigment cells through epidermis as suggested by Hendrick et al. (2019). Examination of the differentiation program and migratory behavior of the different chromatophore lineages could provide crucial insights into these questions.

Similarly to body pigmentation, the developmental and genetic basis of the vast variation in cichlid facial morphology has been previously investigated in several taxa (Albertson & Kocher, 2006; Conith et al., 2018; Kocher et al., 1993; Powder et al., 2014, 2015; Woltering et al., 2018). Our results expand this sampling by the addition of three species occupying distinct positions on the ecomorphological axis, including the generalist, ancestor-like AC. Considering the vast temporal variability between our study species and in contrast to previous studies, we primarily focused on comparison of the developmental (stage), rather than chronological (dpf), stages of cartilage formation. The (overall) craniofacial ontogenies were conserved among sampled species with homologous elements forming in the same order.

The ontogeny was the primary axis of shape variation between species in both examined aspects of craniofacial shapes, indicating that the differences between developmental stages exceeded those present between species. Nonetheless, the morphological differences between species were detected from the onset of chondrogenesis in stage-wise comparisons. Notably, these revealed that both lateral and ventral aspects followed an interesting trend where initially distinct phenotypes (st. 18) converge toward one another (st. 19) to diverge again (st. 20) in morphospace.

Overall, our results are largely consistent with Powder et al. (2015) who also reported the ontogeny to be the main determinant of the cichlid craniofacial development in six Malawi species. Within that ontogenetic framework, based on comparisons using chronological age (expressed in dpf), the authors identified heterochronies as one of the drivers of species-specific phenotypes. By using a complementary approach of stage-wise comparisons, we provide evidence that the differences in craniofacial development exist as soon as cartilage forms, irrespective of the influence of heterochrony.

In conclusion, our results add further evidence that the divergence of developmental trajectories for both hyper-diverse cichlid morphologies of the craniofacial complex and skin pigmentation is specified during early embryonic development, before the overt formation of the trait. Moreover, the variability in developmental processes, exemplified here as heterochronic shifts in chromatophore appearance and morphogenesis of the chondrocranium, acts within conserved frameworks (e.g., following a conserved order of events) to contribute to species-specific phenotypes. The common embryonic origin of pigmentation and craniofacial phenotypes suggests that the differences observed at the onset of overt trait appearance may result from variation occurring during the formation, migration, and differentiation of the NC. In that scenario, we would expect that the subpopulations of the NC differentiating into the cartilage and pigment cell lineages to follow species-specific developmental trajectories, manifested for instance as differential migratory patterns of these cells, sizes of progenitor pools or heterochronies. Thus far, Powder et al. (2014) have reported that the alternate short and long jaw morphologies of *Labeotropheus fuelleborni* and *Maylandia zebra* (Lake Malawi), respectively, are associated with a nonsynonymous mutation in the *limb bud and heart homolog* (*lbh*) gene. This mutation was demonstrated experimentally to result in altered migration patterns of the NCCs in *D. rerio* and *Xenopus*. Similarly, differential expression levels of *pax3a*, mediating xanthophore specification from the NC (Minchin & Hughes, 2008), have been implicated in continuous variation in color patterns in *L. fuelleborni* and *Tropheops* "red cheek" (Lake Malawi) (Albertson et al., 2014). Despite the compelling evidence suggesting the role of NC in the morphological diversity of cichlids, the innate patterns of NCC migration, as well as more general features of the NC development, remain to be explored in the cichlid system (Brandon et al., 2022).

## 5 | CONCLUSIONS: THE USE OF CICHLIDS AS A MODEL FOR EXPERIMENTAL EVO-DEVO

Recent years have seen an increased interest in adopting cichlid fishes as an experimental model system. Despite the considerable advances, several aspects of fundamental

cichlid biology, especially concerning embryonic development, have been largely overlooked. This study highlights the potential of East African cichlids as a valuable addition to the existing repertoire of teleost models, especially for research questions concerning the evolution of embryogenesis, such as axial development and patterning, as well as variability in the development of NC-derived traits. This variation, in turn, suggests that the differences in NC development may underlie the trait diversity. Considering the vast inter- and intraspecific diversity of cichlid fishes, we are certain that cichlid comparative embryology will provide important insights into vertebrate development and evolution.

## AUTHOR CONTRIBUTIONS

Aleksandra Marconi and M. Emília Santos conceived the project and designed the experiments. Aleksandra Marconi, Cassandra Zie Yang, and Samuel McKay performed the experiments and Aleksandra Marconi analysed the data. Aleksandra Marconi wrote the manuscript with contributions or feedback from all authors. All authors read and approved the final version of the manuscript.

## ACKNOWLEDGMENTS

The authors thank Dr. J. Andrew Gillis for help with histology and Dr. Lewis Thomson for technical assistance with sample collection as well as the staff working in the animal facility in Madingley for maintenance of fish stocks. The authors thank Dr. G. Turner (Bangor University) and Dr. D. Joyce and Alan Smith (University of Hull) for the kind gifts of fish stocks. The authors also thank Bethan Clark for valuable comments on the manuscript and the Zoology Imaging Facility for assistance and support with microscopy. Aleksandra Marconi was supported by the Wellcome Trust PhD Programme in Developmental Mechanisms (215223/Z/19/Z). M. Emília Santos was supported by a Natural Environment Research Council Independent Research Fellowship (NE/R01504X/1).

## CONFLICT OF INTEREST STATEMENT

The authors declare no conflict of interest.

## DATA AVAILABILITY STATEMENT

The data that support the findings of this study will be made openly available upon acceptance and before publication.

## ORCID

*Aleksandra Marconi* http://orcid.org/0000-0001-8481-9336
*M. Emília Santos* http://orcid.org/0000-0003-3158-7935

## REFERENCES

Abzhanov, A., Protas, M., Grant, B. R., Grant, P. R., & Tabin, C. J. (2004). *Bmp4* and morphological variation of beaks in Darwin's finches. *Science*, *305*, 1462–1465. https://doi.org/10.1126/science.1098095.

Alberch, P., Gould, S. J., Oster, G. F., & Wake, D. B. (1979). Size and shape in ontogeny and phylogeny. *Paleobiology*, *5*, 296–317.

Albertson, R. C., & Kocher, T. D. (2006). Genetic and developmental basis of cichlid trophic diversity. *Heredity*, *97*, 211–221. https://doi.org/10.1038/sj.hdy.6800864

Albertson, R. C., Powder, K. E., Hu, Y., Coyle, K. P., Roberts, R. B., & Parsons, K. J. (2014). Genetic basis of continuous variation in the levels and modular inheritance of pigmentation in cichlid fishes. *Molecular Ecology*, *23*, 5135–5150. https://doi.org/10.1111/mec.12900

Balon, E. K. (1977). Early ontogeny of *Labeotropbeus* Ahl, 1927 (Mbuna, Cichlidae, Lake Malawi), with a discussion on advanced protective styles in fish reproduction and development. *Environmental Biology of Fishes*, *2*, 147–176. https://doi.org/10.1007/BF00005370

Balon, E. K. (1999). Alternative ways to become a juvenile or a definitive phenotype (and on some persisting linguistic offenses). *Environmental Biology of Fishes*, *56*(1–2), 17–38. https://doi.org/10.1023/a:1007502209082

Brandon, A. A., Almeida, D., & Powder, K. E. (2022). Neural crest cells as a source of microevolutionary variation. *Seminars in Cell & Developmental Biology*. https://doi.org/10.1016/j.semcdb.2022.06.001

Bronner, M. E., & LeDouarin, N. M. (2012). Development and evolution of the neural crest: An overview. *Developmental Biology*, *366*, 2–9. https://doi.org/10.1016/j.ydbio.2011.12.042

Bronner, M. E., & Simões-Costa, M. (2016). The neural crest migrating into the twenty-first century. In P. M. Wassarman (Ed.), *Current topics in developmental biology* (pp. 115–134). Academic Press.

Brzozowski, F., Roscoe, J., Parsons, K., & Albertson, C. (2012). Sexually dimorphic levels of color trait integration and the resolution of sexual conflict in Lake Malawi cichlids. *Journal of Experimental Zoology Part B: Molecular and Developmental Evolution*, *318*, 268–278. https://doi.org/10.1002/jez.b.22443

Clark, B., Elkin, J., Marconi, A., Turner, G. F., Smith, A. M., Joyce, D., Miska, E. A., Juntti, S. A., & Santos, M. E. (2022). *Oca2* targeting using CRISPR/Cas9 in the Malawi cichlid *Astatotilapia calliptera*. *Royal Society Open Science*, *9*, 220077. https://doi.org/10.1098/rsos.220077

Conith, M. R., Hu, Y., Conith, A. J., Maginnis, M. A., Webb, J. F., & Albertson, R. C. (2018). Genetic and developmental origins of a unique foraging adaptation in a Lake Malawi cichlid genus. *Proceedings of the National Academy of Sciences*, *115*, 7063–7068. https://doi.org/10.1073/pnas.1719798115

de Jong, I. M. L., Witte, F., & Richardson, M. K. (2009). Developmental stages until hatching of the Lake Victoria cichlid *Haplochromis piceatus* (Teleostei: Cichlidae). *Journal of Morphology*, *270*, 519–535. https://doi.org/10.1002/jmor.10716

Devoto, S. H., Stoiber, W., Hammond, C. L., Steinbacher, P., Haslett, J. R., Barresi, M. J., Patterson, S. E., Adiarte, E. G., & Hughes, S. M. (2006). Generality of vertebrate developmental patterns: evidence for a dermomyotome in fish. *Evolution &*

*Development*, *8*, 101–110. https://doi.org/10.1111/j.1525-142X.2006.05079.x

Douarin, N. L., & Kalcheim, C. (1999). *The neural crest*. Cambridge University Press.

Eccles, D., & Trewavas, E. (1989). *Malawian cichlid fishes: The classification of some haplochromine genera*. Herten.

Eom, D. S., Inoue, S., Patterson, L. B., Gordon, T. N., Slingwine, R., Kondo, S., Watanabe, M., & Parichy, D. M. (2012). Melanophore migration and survival during zebrafish adult pigment stripe development require the immunoglobulin superfamily adhesion molecule Igsf11. *PLoS Genetics*, *8*, e1002899. https://doi.org/10.1371/journal.pgen.1002899

Fujimura, K., & Okada, N. (2007). Development of the embryo, larva and early juvenile of Nile tilapia *Oreochromis niloticus* (Pisces: Cichlidae). developmental staging system. *Development, Growth & Differentiation*, *49*, 301–324. https://doi.org/10.1111/j.1440-169X.2007.00926.x

Genner, M. J., & Turner, G. F. (2005). The mbuna cichlids of Lake Malawi: A model for rapid speciation and adaptive radiation. *Fish and Fisheries*, *6*, 1–34. https://doi.org/10.1111/j.1467-2679.2005.00173.x

Hendrick, L. A., Carter, G. A., Hilbrands, E. H., Heubel, B. P., Schilling, T. F., & Le Pabic, P. (2019). Bar, stripe and spot development in sand-dwelling cichlids from Lake Malawi. *EvoDevo*, *10*, 18. https://doi.org/10.1186/s13227-019-0132-7

Henning, F., & Meyer, A. (2014). The evolutionary genomics of cichlid fishes: Explosive speciation and adaptation in the postgenomic era. *Annual Review of Genomics and Human Genetics*, *15*, 417–441. https://doi.org/10.1146/annurev-genom-090413-025412

Holley, S. A. (2007). The genetics and embryology of zebrafish metamerism. *Developmental Dynamics*, *236*, 1422–1449. https://doi.org/10.1002/dvdy.21162

Hubaud, A., & Pourquié, O. (2014). Signalling dynamics in vertebrate segmentation. *Nature Reviews Molecular Cell Biology*, *15*, 709–721. https://doi.org/10.1038/nrm3891

Jones, A. J. (1972). The early development of substrate-brooding cichlids (Teleostei: Cichlidae) with a discussion of a new system of staging. *Journal of Morphology*, *136*, 255–272. https://doi.org/10.1002/jmor.1051360302

Jones, K. E., Angielczyk, K. D., Polly, P. D., Head, J. J., Fernandez, V., Lungmus, J. K., Tulga, S., & Pierce, S. E. (2018). Fossils reveal the complex evolutionary history of the mammalian regionalized spine. *Science*, *361*, 1249–1252. https://doi.org/10.1126/science.aar3126

Juntti, S. A., Hu, C. K., & Fernald, R. D. (2013). Tol2-mediated generation of a transgenic haplochromine cichlid, *Astatotilapia burtoni*. *PLoS One*, *8*, e77647. https://doi.org/10.1371/journal.pone.0077647

Kimmel, C. B., Ballard, W. W., Kimmel, S. R., Ullmann, B., & Schilling, T. F. (1995). Stages of embryonic development of the zebrafish. *Developmental Dynamics*, *203*, 253–310. https://doi.org/10.1002/aja.1002030302

Klingenberg, C. P. (2011). MorphoJ: an integrated software package for geometric morphometrics. *Molecular Ecology Resources*, *11*, 353–357. https://doi.org/10.1111/j.1755-0998.2010.02924.x

Kocher, T. D. (2004). Adaptive evolution and explosive speciation: the cichlid fish model. *Nature Reviews Genetics*, *5*, 288–298. https://doi.org/10.1038/nrg1316

Kocher, T. D., Conroy, J. A., McKaye, K. R., & Stauffer, J. R. (1993). Similar morphologies of cichlid fish in Lakes Tanganyika and Malawi are due to convergence. *Molecular Phylogenetics and Evolution*, *2*, 158–165. https://doi.org/10.1006/mpev.1993.1016

Kratochwil, C. F., Kautt, A. F., Nater, A., Härer, A., Liang, Y., Henning, F., & Meyer, A. (2022). An intronic transposon insertion associates with a trans-species color polymorphism in Midas cichlid fishes. *Nature Communications*, *13*, 296. https://doi.org/10.1038/s41467-021-27685-8

Kratochwil, C. F., Liang, Y., Gerwin, J., Woltering, J. M., Urban, S., Henning, F., Machado-Schiaffino, G., Hulsey, C. D., & Meyer, A. (2018). Agouti-related peptide 2 facilitates convergent evolution of stripe patterns across cichlid fish radiations. *Science*, *362*, 457–460. https://doi.org/10.1126/science.aao6809

Kratochwil, C. F., Sefton, M. M., & Meyer, A. (2015). Embryonic and larval development in the Midas cichlid fish species flock (Amphilophus spp.): A new evo-devo model for the investigation of adaptive novelties and species differences. *BMC Developmental Biology*, *15*, 12. https://doi.org/10.1186/s12861-015-0061-1

Li, C.-Y., Steighner, J. R., Sweatt, G., Thiele, T. R., & Juntti, S. A. (2021). Manipulation of the Tyrosinase gene permits improved CRISPR/Cas editing and neural imaging in cichlid fish. *Scientific Reports*, *11*, 15138. https://doi.org/10.1038/s41598-021-94577-8

Liang, Y., Gerwin, J., Meyer, A., & Kratochwil, C. F. (2020). Developmental and cellular basis of vertical bar color patterns in the East African cichlid fish *Haplochromis latifasciatus*. *Frontiers in Cell and Developmental Biology*, *8*, 62. https://doi.org/10.3389/fcell.2020.00062

Lindell, L. E. (1994). The evolution of vertebral number and body size in snakes. *Functional Ecology*, *8*, 708–719. https://doi.org/10.2307/2390230

Loh, Y.-H. E., Katz, L. S., Mims, M. C., Kocher, T. D., Yi, S. V., & Streelman, J. T. (2008). Comparative analysis reveals signatures of differentiation amid genomic polymorphism in Lake Malawi cichlids. *Genome Biology*, *9*, R113. https://doi.org/10.1186/gb-2008-9-7-r113

Loring, J. F., & Erickson, C. A. (1987). Neural crest cell migratory pathways in the trunk of the chick embryo. *Developmental Biology*, *121*, 220–236. https://doi.org/10.1016/0012-1606(87)90154-0

Lowery, L. A., & Sive, H. (2004). Strategies of vertebrate neurulation and a re-evaluation of teleost neural tube formation. *Mechanisms of Development*, *121*, 1189–1197. https://doi.org/10.1016/j.mod.2004.04.022

Malinsky, M., Challis, R. J., Tyers, A. M., Schiffels, S., Terai, Y., Ngatunga, B. P., Miska, E. A., Durbin, R., Genner, M. J., & Turner, G. F. (2015). Genomic islands of speciation separate cichlid ecomorphs in an East African crater lake. *Science*, *350*, 1493–1498. https://doi.org/10.1126/science.aac9927

Malinsky, M., Svardal, H., Tyers, A. M., Miska, E. A., Genner, M. J., Turner, G. F., & Durbin, R. (2018). Whole-genome sequences of Malawi cichlids reveal multiple radiations interconnected by gene flow. *Nature Ecology & Evolution*, *2*(12), 1940–1955. https://doi.org/10.1038/s41559-018-0717-x

McKinney, M. L., & McNamara, K. J. (1992). Heterochrony. The evolution of ontogeny. *Geological Magazine*, *129*, 646–647. https://doi.org/10.1017/S0016756800021919

Meyer, A. (1993). Phylogenetic relationships and evolutionary processes in East African cichlid fishes. *Trends in Ecology & Evolution*, *8*, 279–284. https://doi.org/10.1016/0169-5347(93)90255-N

Meyer, A., Kocher, T. D., Basasibwaki, P., & Wilson, A. C. (1990). Monophyletic origin of Lake Victoria cichlid fishes suggested by mitochondrial DNA sequences. *Nature*, *347*, 550–553. https://doi.org/10.1038/347550a0

Minchin, J. E. N., & Hughes, S. M. (2008). Sequential actions of Pax3 and Pax7 drive xanthophore development in zebrafish neural crest. *Developmental Biology*, *317*, 508–522. https://doi.org/10.1016/j.ydbio.2008.02.058

Moran, P., & Kornfield, I. (1993). Retention of an ancestral polymorphism in the Mbuna species flock (Teleostei: Cichlidae) of Lake Malawi. *Molecular Biology and Evolution*, *10*, 1015. https://doi.org/10.1093/oxfordjournals.molbev.a040063

Morin-Kensicki, E. M., Melancon, E., & Eisen, J. S. (2002). Segmental relationship between somites and vertebral column in zebrafish. *Development*, *129*, 3851–3860. https://doi.org/10.1242/dev.129.16.3851

Morrison, C. M., Miyake, T., & Wright, J. R. (2001). Histological study of the development of the embryo and early larva of *Oreochromis niloticus* (Pisces: Cichlidae). *Journal of Morphology*, *247*, 172–195. https://doi.org/10.1002/1097-4687(200102)247:2<172::AID-JMOR1011>3.0.CO;2-H

Müller, J., Scheyer, T. M., Head, J. J., Barrett, P. M., Werneburg, I., Ericson, P. G. P., Pol, D., & Sánchez-Villagra, M. R. (2010). Homeotic effects, somitogenesis and the evolution of vertebral numbers in recent and fossil amniotes. *Proceedings of the National Academy of Sciences*, *107*, 2118–2123. https://doi.org/10.1073/pnas.0912622107

Otten, E. (1981). The development of a mouth-opening mechanism in a generalized haplochromis species: H. Elegans Trewavas 1933 (Pisces, Cichlidae). *Netherlands Journal of Zoology*, *32*(1), 31–48. https://doi.org/10.1163/002829682x00021

Patterson, L. B., & Parichy, D. M. (2019). Zebrafish pigment pattern formation: Insights into the development and evolution of adult form. *Annual Review of Genetics*, *53*, 505–530. https://doi.org/10.1146/annurev-genet-112618-043741

Powder, K. E., & Albertson, R. C. (2016). Cichlid fishes as a model to understand normal and clinical craniofacial variation. *Developmental Biology*, *415*, 338–346. https://doi.org/10.1016/j.ydbio.2015.12.018

Powder, K. E., Cousin, H., McLinden, G. P., & Craig Albertson, R. (2014). A nonsynonymous mutation in the transcriptional regulator *lbh* is associated with cichlid craniofacial adaptation and neural crest cell development. *Molecular Biology and Evolution*, *31*, 3113–3124. https://doi.org/10.1093/molbev/msu267

Powder, K. E., Milch, K., Asselin, G., & Albertson, R. C. (2015). Constraint and diversification of developmental trajectories in cichlid facial morphologies. *EvoDevo*, *6*, 25. https://doi.org/10.1186/s13227-015-0020-8

R Core Team. (2022). R: A language and environment for statistical computing. R Foundation for Statistical Computing, Vienna, Austria. https://www.R-project.org/.

Richardson, M. K., Allen, S. P., Wright, G. M., Raynaud, A., & Hanken, J. (1998). Somite number and vertebrate evolution. *Development*, *125*, 151–160. https://doi.org/10.1242/dev.125.2.151

Roberts, R. B., Moore, E. C., & Kocher, T. D. (2017). An allelic series at pax7a is associated with colour polymorphism diversity in Lake Malawi cichlid fish. *Molecular Ecology*, *26*, 2625–2639. https://doi.org/10.1111/mec.13975

Rocha, M., Singh, N., Ahsan, K., Beiriger, A., & Prince, V. E. (2020). Neural crest development: Insights from the zebrafish. *Developmental Dynamics*, *249*, 88–111. https://doi.org/10.1002/dvdy.122

Rohlf, F. (2010). *TpsDig2: digitize coordinates of landmarks and capture outlines*. Department of Ecology & Evolution, Stony Brook University, Stony Brook. NY, USA.

Saemi-Komsari, M., Salehi, M., Mansouri-Chorehi, M., Eagderi, S., & Mousavi-Sabet, H. (2018). Developmental morphology and growth patterns of laboratory-reared giraffe cichlid, *Nimbochromis venustus* boulenger, 1908. *International Journal of Aquatic Biology*. *6*, 170–178. https://doi.org/10.22034/ijab.v6i3.525

Salzburger, W. (2018). Understanding explosive diversification through cichlid fish genomics. *Nature Reviews Genetics*, *19*, 705–717. https://doi.org/10.1038/s41576-018-0043-9

Santos, M. E., Braasch, I., Boileau, N., Meyer, B. S., Sauteur, L., Böhne, A., Belting, H.-G., Affolter, M., & Salzburger, W. (2014). The evolution of cichlid fish egg-spots is linked with a *cis*-regulatory change. *Nature Communications*, *5*, 5149. https://doi.org/10.1038/ncomms6149

Schindelin, J., Arganda-Carreras, I., Frise, E., Kaynig, V., Longair, M., Pietzsch, T., Preibisch, S., Rueden, C., Saalfeld, S., Schmid, B., Tinevez, J. Y., White, D. J., Hartenstein, V., Eliceiri, K., Tomancak, P., & Cardona, A. (2012). Fiji: An open-source platform for biological-image analysis. *Nature Methods*, *9*, 676–682. https://doi.org/10.1038/nmeth.2019

Schröter, C., Herrgen, L., Cardona, A., Brouhard, G. J., Feldman, B., & Oates, A. C. (2008). Dynamics of zebrafish somitogenesis. *Developmental Dynamics*, *237*, 545–553. https://doi.org/10.1002/dvdy.21458

Sela-Donenfeld, D., & Kalcheim, C. (2000). Inhibition of noggin expression in the dorsal neural tube by somitogenesis: A mechanism for coordinating the timing of neural crest emigration. *Development*, *127*, 4845–4854. https://doi.org/10.1242/dev.127.22.4845

Stickney, H. L., Barresi, M. J. F., & Devoto, S. H. (2000). Somite development in zebrafish. *Developmental Dynamics*, *219*, 287–303. https://doi.org/10.1002/1097-0177(2000)9999:9999<::AID-DVDY1065>3.0.CO;2-A

Takahashi, G., & Kondo, S. (2008). Melanophores in the stripes of adult zebrafish do not have the nature to gather, but disperse when they have the space to move. *Pigment Cell & Melanoma Research*, *21*, 677–686. https://doi.org/10.1111/j.1755-148X.2008.00504.x

Teillet, M.-A., Kalcheim, C., & Le Douarin, N. M. (1987). Formation of the dorsal root ganglia in the avian embryo: Segmental origin and migratory behavior of neural crest progenitor cells. *Developmental Biology*, *120*, 329–347. https://doi.org/10.1016/0012-1606(87)90236-3

Torres-Paz, J., Leclercq, J., & Rétaux, S. (2019). Maternally regulated gastrulation as a source of variation contributing to cavefish forebrain evolution. *eLife*, *8*, e50160. https://doi.org/10.7554/eLife.50160.

Woltering, J. M., Holzem, M., Schneider, R. F., Nanos, V., & Meyer, A. (2018). The skeletal ontogeny of *Astatotilapia burtoni*—a direct-

developing model system for the evolution and development of the teleost body plan. *BMC Developmental Biology*, *18*, 8. https://doi.org/10.1186/s12861-018-0166-4.S

## SUPPORTING INFORMATION

Additional supporting information can be found online in the Supporting Information section at the end of this article.

**How to cite this article:** Marconi, A., Yang, C. Z., McKay, S., & Santos, M. E. (2023). Morphological and temporal variation in early embryogenesis contributes to species divergence in Malawi cichlid fishes. *Evolution & Development*, 25, 170–193. https://doi.org/10.1111/ede.12429